Light diffusion and diffusing-wave spectroscopy in nematic liquid crystals

H. Stark, M. H. Kao, K. A. Jester, T. C. Lubensky, and A. G. Yodh

Department of Physics and Astronomy, University of Pennsylvania, Philadelphia, Pennsylvania 19104

P. J. Collings

Department of Physics, Swarthmore College, Swarthmore, Pennsylvania 19081

We present a detailed theoretical, experimental, and numerical study of light diffusion and diffusing-wave spectroscopy in nematic liquid crystals. We report on experiments showing that the transport of light energy is governed by an anisotropic correlation diffusion equation, and we measure the parallel and the perpendicular components of the diffusion tensor and the diffusing-wave spectroscopy temporal decay rate. We derive theoretically the correlation diffusion equations. We then calculate the diffusing-wave spectroscopy temporal decay rate, and we provide explicit approximate, yet accurate, expressions for the components of the light diffusion tensor, which we evaluate numerically as a function of material parameters of nematics. Using the actual scattering cross sections for a nematic, we simulate photon transport and verify that it is described at long times by an anisotropic diffusion equation with diffusion coefficients in excellent agreement with both those obtained experimentally and those obtained from our analytical expressions. © 1997 Optical Society of America. [S0740-3232(97)03001-9]

1. INTRODUCTION

A. Overview of Multiple Scattering

During the past decade we have witnessed the rapid growth of an interdisciplinary field of optical research aimed at understanding and using the phenomenologies associated with highly scattered light in turbid media. Recent fundamental advances include, for example, the discoveries of coherent backscattering[1,2] and hidden correlations[3] in disordered media, studies of photon localization,[4] the theory and the creation of photonic band-gap materials,[5] investigations of light diffusion in highly scattering media with photon gain,[6] and the development and the application of diffusing-wave spectroscopy (DWS),[2,7–9] whereby temporal correlations of highly scattered light probe dynamical motions in homogeneous complex fluids such as colloids,[10] foams,[11] emulsions,[12] and gels,[13] as well as in heterogenous complex fluids and tissues.[14]

In addition, although light has been used to investigate the interior of the human body for many years,[15] the recent recognition and the widespread acceptance that light transport over long distances in human tissues is well approximated as a diffusive process have led to the use of diffusing near-infrared photons[16] to view body function and structure in deep tissues. With this basic physical model, it is possible to separate quantitatively tissue scattering effects from tissue absorption effects and to incorporate accurately the effects of boundaries.[17] Waves of diffuse light energy density[18] (and their time-domain analogs[19]) propagate deeply in tissues while obeying simple optical rules such as refraction,[20] diffraction,[21] interference,[22] and dispersion[23] as they encounter variations in tissue optical properties. Finally, functional imaging and spectroscopic techniques that use these diffusing photons are being explored for such applications as the detection of brain bleeds,[24] the quantification of oxygen saturation in the brain,[25] the study of mitochondrial diseases,[26] and the detection of breast tumors.[27]

To date, virtually all media studied with diffusing light have been isotropic. In media, such as muscle tissue, that are not isotropic, quantification of light signals is still accomplished with isotropic physical models. In this paper we investigate the nature of light diffusion and correlation transport through orientationally ordered turbid materials. A preliminary report of the work appears in Ref. 28. We are interested in understanding the manifestations of these directional correlations on light diffusion and on the transport of higher-order correlation functions such as the temporal electric-field autocorrelation function. We provide rigorous theoretical predictions about these issues, and we corroborate them with extensive experimental and computational evidence. We have focused on the specific case of light transport through turbid nematic liquid crystals to address these phenomena. An alternative theoretical treatment for general anisotropic media appears in Refs. 28 and 29.

Nematic liquid crystals are composed of rod-shaped molecules that are translationally disordered but that align on average along a common direction. The preferred direction is described by a unit vector **n** called the director. As a result of these directional correlations, nematics present interesting complications for light diffusion that extend beyond isotropic, random media. The optical properties of nematic liquid crystals are highly anisotropic.[30,31] The speed of light with electric polarization perpendicular to the director differs from that with polarization in the plane of the director and the propaga-

tion wave vector. The light-scattering cross sections, which originate from local director fluctuations, depend on the directions of the electric field and the propagation vectors with respect to the average molecular orientation. Furthermore, nematic liquid crystals strongly scatter visible light; samples with thicknesses greater than a few millimeters appear milky white, and, by analogy with milky-white colloids and foams, one might expect that photons diffuse through these media. Indeed, in two elegant recent papers,[32,33] coherent backscattering from turbid nematics has been observed.

Our paper is organized as follows. In the remainder of Section 1 we present the basic theoretical ideas that underly light diffusion and correlation transport in nematic liquid crystals, and we present our experimental results. In particular, we write down the diffusion equation for light transport in the nematic liquid crystal and provide expressions for the photon diffusion coefficients parallel and perpendicular to the director. We also provide an explicit formulation, analogous to that of DWS in isotropic media, for the temporal electric-field autocorrelation function of the diffused speckle. The experiments are then presented and analyzed with this formalism. In Section 2 we present a rigorous derivation of the main theoretical results: We establish an explicit connection to previous studies in isotropic media and describe some predictions for some as yet unobserved phenomena. Finally, we present computer simulations that amplify and enlarge the scope of our experimental and theoretical observations. In a series of appendixes, we provide the derivations with technical details of results used in Section 2. In Appendix A we calculate the photon Green function in the weak-scattering limit. In Appendix B we derive a path-integral formulation for photon diffusion in nematic liquid crystals. In Appendix C we calculate the mean-square displacements per photon scattering step for directions parallel and perpendicular to the director, and in Appendix D we display the complete structure factor that determines scattering cross sections in nematic liquid crystals.

B. Diffusing-Wave Spectroscopy in a Nematic Liquid Crystal

Nematic liquid crystals are uniaxial fluids[30,31] with bar-like molecules aligned on average along a local anisotropy axis specified by the unit Frank director $\mathbf{n}(\mathbf{r}, t)$, as depicted schematically in Fig. 1. The equilibrium director
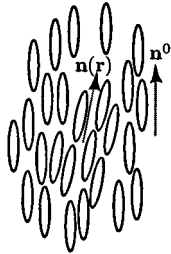

Fig. 1. Schematic representation of a nematic liquid crystal showing molecules aligned on average along the local Frank director $\mathbf{n}(\mathbf{r}, t)$ and the equilibrium director $\mathbf{n}_0$.

$\mathbf{n}^0$ is spatially uniform. Thus nematics are birefringent,[34,35] with light wave vector $\mathbf{k}$ propagating in ordinary rays, with electric polarization perpendicular to both wave vectors $\mathbf{k}$ and $\mathbf{n}_0$, and in extraordinary rays, with polarization in the plane defined by $\mathbf{k}$ and $\mathbf{n}^0$. The velocities of the ordinary and the extraordinary rays are different, and the velocity of the extraordinary ray depends on the angle between $\mathbf{k}$ and $\mathbf{n}^0$.

Linear deviations $\delta\mathbf{n}(\mathbf{r}, t)$ of the director are perpendicular to $\mathbf{n}_0$. Since there is no energy cost associated with a uniform rotation, fluctuations in $\mathbf{n}(\mathbf{r})$ diverge at small wave vector $\mathbf{q}$ in the absence of external aligning fields: $\langle |\delta n(\mathbf{q})|^2 \rangle \sim T/Kq^2$, where T is the temperature and K is a Frank elastic constant, which depends on the direction of $\mathbf{q}$ relative to $\mathbf{n}^0$. In addition, there are long-wavelength, low-frequency diffusive hydrodynamic modes with characteristic frequency $\Gamma_{\mathbf{q}} \sim Kq^2/\eta$, where η is a viscosity, which depends, like K, on the direction of $\mathbf{q}$. The time-dependent fluctuations in $\delta\mathbf{n}(\mathbf{q}, t)$ are proportional to $(T/Kq^2)\exp(-\Gamma_{\mathbf{q}}t)$. The direction of local dielectric anisotropy is parallel to $\mathbf{n}(\mathbf{r}, t)$, so fluctuations in $\mathbf{n}$ lead to fluctuations in the dielectric tensor ϵ_{ij}. Fluctuations in ϵ_{ij} scatter light with cross section proportional to

$$B(\mathbf{q}, t) \sim (\Delta\epsilon)^2(\omega/c)^4(T/Kq^2)\exp(-\Gamma_{\mathbf{q}}t), \quad (1.2.1)$$

where $\Delta\epsilon = \epsilon_\parallel - \epsilon_\perp$ is the dielectric anisotropy, ω is the angular frequency of light, and c is the velocity of light. The long-wavelength divergence of $B(\mathbf{q}, t)$ causes light to scatter much more strongly in a nematic liquid crystal than in an isotropic fluid, where fluctuations in ϵ_{ij} are produced by fluctuations in the density. This form of $B(\mathbf{q}, t)$ should be contrasted with its form, $B(\mathbf{q}, t) = |F(\mathbf{q})|^2 S(\mathbf{q}, 0)\exp(-D_s q^2 t)$, in a dilute colloidal suspension,[7,8] where $|\mathbf{F}(\mathbf{q})|^2$ is the particle form factor, $S(\mathbf{q}, 0)$ is the static structure factor, and D_s is the self-diffusion constant of the colloidal particles. Although the structure factor has interesting behavior at wavelengths of the order of the spacing between particles, it does not diverge as $\mathbf{q} \to 0$. The dynamics of the liquid-crystal and the colloidal systems are both diffusive. The frequency $\Gamma_{\mathbf{q}}$ in a nematic is, however, explicitly proportional to the static structure factor T/Kq^2, whereas D_s need not depend on $S(\mathbf{q}, 0)$.

A typical path of light rays in a large nematic sample is depicted in Fig. 2. There is a series of steps, with an average length equal to a mean free path l between scattering events that alter the direction of light propagation. At length scales greater than the scattering mean free path $l^* > l$, there is no correlation between step directions, and transport becomes diffusive. Nematic liquid crystals are uniaxial, so the light-energy density $\mathbf{E} \cdot \epsilon^0 \mathbf{E}$ will obey an anisotropic diffusion equation. More generally, the time-dependent electric-field autocorrelation function $\mathcal{G}(\mathbf{R}, T, t) = \langle \mathbf{E}(\mathbf{R}, T + t/2) \cdot \epsilon^0 \mathbf{E}(\mathbf{R}, T - t/2) \rangle$ measured in DWS experiments obeys an anisotropic diffusion equation with a dynamical absorption coefficient $\mu(t)$:

$$\left[\frac{\partial}{\partial T} - D_\parallel \nabla_\parallel{}^2 - D_\perp \nabla_\perp{}^2 + \mu(t) \right] \mathcal{G}(\mathbf{R}, T, t) = \tilde{J}(\mathbf{R}, T),$$
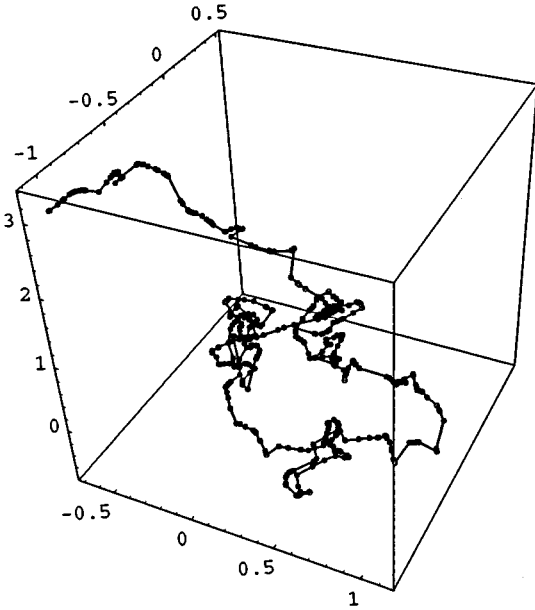$$(1.2.2)$$

Fig. 2. Typical photon path in a nematic, obtained from our numerical simulations. Note that there are many short steps with small angle changes between steps.

where $\widetilde{J}(\mathbf{R}, T)$ is a source term and $D_\parallel$ and $D_\perp$ are, respectively, the photon diffusion coefficients for directions parallel and perpendicular to $\mathbf{n}_0$. In isotropic systems the single photon diffusion constant D can be expressed as $D = (1/6)\langle R^2\rangle/\langle T\rangle$, where $\langle T\rangle$ is the average time and $\langle R^2\rangle$ is the mean-square photon displacement per step. The angle brackets $\langle\ \rangle$ here denote an average over all the random paths of the diffusing photon. When there is a single light velocity $\bar{c}$, $\langle T\rangle = l/\bar{c}$. In addition, in isotropic systems, $\langle R^2\rangle = 2ll^*$, where the ratio l/l^* of the mean free path to the transport mean free path is equal to $\langle 1 - \cos\theta\rangle$, where θ is the change in angle between input and output directions at a scattering event. Thus in isotropic systems

$$D = \frac{1}{6}\frac{\langle R^2\rangle}{\langle T\rangle} = \frac{1}{3}\bar{c}l^*. \qquad (1.2.3)$$

In anisotropic systems, mean free paths depend on polarization and direction of propagation. The average time between collisions $\langle T\rangle$ and the mean-square displacements per step $\langle R_\parallel^2\rangle$ and $\langle R_\perp^2\rangle$ for respective directions parallel and perpendicular to $\mathbf{n}^0$ are, however, well defined, and

$$D_\parallel = \frac{1}{2}\frac{\langle R_\parallel^2\rangle}{\langle T\rangle}, \quad D_\perp = \frac{1}{4}\frac{\langle R_\perp^2\rangle}{\langle T\rangle}. \qquad (1.2.4)$$

As we show below, the mean free path for the extraordinary ray tends to zero as the external magnetic field $\mathbf{H}$ aligning the director tends to zero. It is nonetheless possible to define an average scattering mean free path $\bar{l}$, an average speed of light $\bar{c}$, and parallel and perpendicular transport mean free paths $l_\parallel^*$ and $l_\perp^*$ that are finite in the $\mathbf{H} \to 0$ limit, such that $\langle R_\parallel^2\rangle = (2/3)\bar{l}l_\parallel^*$ and $\langle R_\perp^2\rangle = (4/3)\bar{l}l_\perp^*$. Then $D_\parallel = \bar{c}l_\parallel^*/3$ and $D_\perp = \bar{c}l_\perp^*/3$. In Subsection 2.E we derive an analytic expression for $\langle T\rangle$ in

terms of $B(\mathbf{q}, t)$ and the indices of refraction of the nematic. Exact analytic expressions for the mean-square displacements $\langle R_\parallel^2\rangle$ and $\langle R_\perp^2\rangle$ cannot be obtained here. Excellent approximations to these quantities are, however, derived in Appendix C. In Refs. 28 and 29 we give the diffusion constants in a form that involves the inversion of an infinite-dimensional matrix. The first in a sequence of approximations is identical to the expressions derived here. The photon diffusion coefficients obtained from these expressions for the nematic liquid-crystal material p-pentyl-p'-cyanobiphenyl (5CB) studied experimentally are $D_\parallel = 1.43 \times 10^9$ cm^2/s and $D_\perp = 0.98 \times 10^9$ cm^2/s, yielding $D_\parallel/D_\perp = 1.45$, in good agreement with experiments.

The dynamic absorption coefficient $\mu(t)$ can be expressed as

$$\mu(t) = \frac{1}{\langle T\rangle}\left\langle\frac{\delta B(t)}{B}\right\rangle, \qquad (1.2.5)$$

where $\delta B(t) = B(0) - B(t)$. In isotropic systems, $\delta B(t) = 2B(0)k_0^2 D_s(l/l^*)t$, where k_0 is the wave number of light, so $\mu(t) = (2\bar{c}/l^*)D_s k_0^2 t$. In nematics, $\delta B(t)/B$ depends only on viscosities and not on elastic constants determining $B(0)$:

$$\mu(t) \sim 2k_B T(\Delta\epsilon)^2\frac{c}{8\pi}\frac{[n^2]}{[n^3]}\frac{\omega^4}{c^4}\left\langle\frac{1}{\eta}\right\rangle t$$

$$= \left[\frac{2k_B T(\Delta\epsilon)^2\omega^4}{9\pi c^3\sqrt{\epsilon_\perp}}\right]\frac{t}{\gamma_{\text{eff}}}, \qquad (1.2.6)$$

where $[n^p]$ is an average over angle and polarization of the pth power of the index of refraction, $\langle(1/\eta)\rangle$ is a weighted average over paths of the inverse viscosity, and γ_{eff} is an effective viscosity, which can be approximated by the rotational viscosity γ. For the nematic compound 5CB, $\gamma = 81$ cycles per second (cps).

In most experiments (including those reported here), a constant-power laser beam illuminates the sample, and the intensity of scattered light is measured at a detector. These experiments measure the T-independent field correlation function $\mathcal{G}(\mathbf{R}, t)$ [i.e., the zero-frequency limit of the Fourier transform of $\mathcal{G}(\mathbf{R}, T, t)$]. The normalized electric-field correlation function measured at the detector is then $g_1(t) = \mathcal{G}(\mathbf{R}, t)/\mathcal{G}(\mathbf{R}, 0)$. It can be expressed as an integral over all the arrival times of the quantity $\exp[-\mu(t)T]$ weighted by the probability $P(\mathbf{R}, T)$ that a diffusing photon arrives at $\mathbf{R}$ in time T:

$$g_1(t) = \int_0^\infty dT P(\mathbf{R}, T)\exp[-\mu(t)T]. \qquad (1.2.7)$$

The diffusive probability can be written as $P(\mathbf{R}, T) = U(\mathbf{R}, T)/\int_0^\infty dT U(\mathbf{R}, T)$, where $U(\mathbf{R}, T)$ satisfies the diffusion equation

$$\left(\frac{\partial}{\partial T} - D_\parallel\nabla_\parallel^2 - D_\perp\nabla_\perp^2\right)U(\mathbf{R}, T) = 0, \qquad (1.2.8)$$
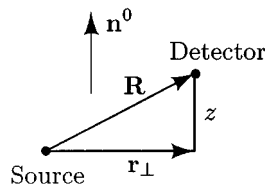
Fig. 3. Idealized geometry for photon diffusion in an anisotropic medium. Shown are the vector $\mathbf{R}$ from the source to the detector and the decomposition of $\mathbf{R}$ into components z and $\mathbf{r}_\perp$ parallel and perpendicular to the director $\mathbf{n}^0$.

subject to boundary conditions defined by the geometry of the experiment. For a point source in an infinite medium,

$$U(\mathbf{R},\,T) = \frac{1}{(4\,\pi|T|)^{3/2}}\,\frac{1}{D_\perp\sqrt{D_\parallel}}$$
$$\times \exp\left[-\frac{1}{4|T|}\left(\frac{|z|^2}{D_\parallel} + \frac{r_\perp{}^2}{D_\perp}\right)\right],$$

(1.2.9)

where z is the component of $\mathbf{R}$ along $\mathbf{n}_0$ and $\mathbf{r}_\perp$ is its component perpendicular to $\mathbf{n}^0$, as shown in Fig. 3.

C. Experimental Results

We performed experiments with 5CB, a nematic liquid crystal with a nematic-to-isotropic transition temperature $T_c = 35\ °\text{C}$. Our experimental setup is shown in Fig. 4. The liquid crystal was housed in a quartz cylindrical cell that was 1 cm thick and 2 cm in diameter. The entire sample was placed in a magnetic field for uniform orientation of the director along the z direction shown in Fig. 4(a). The cylindrical cell rested in a hollow Al frame through which water was circulated from a temperature controlled source, as shown in Fig. 4(c). With the field turned off, the sample was heated to $T = 40\ °\text{C}$, well into its isotropic phase. A magnetic field of 2 kG was then applied. As shown in Fig. 4(b), the magnet produced a field that was uniform to within 5% at 2 kG over the cylindrical region, 3 cm in length and ~ 3 cm in diameter. Because the sample cell could easily fit inside this region, there was relatively little fluctuation in the field strength over the size of the cell. To ensure alignment of the field parallel to the input and output faces of the cell, we placed a Hall probe against the sample face and adjusted the angle of the sample until the field measured was zero. Then the sample was slowly cooled in this magnetic field from the isotropic phase to the nematic phase at $T = 30\ °\text{C}$. We were able to control the temperature of the sample to within $\sim 1°$, even when the sample was illuminated by laser powers of as high as ~ 100 mW. Thus at $30\ °\text{C}$ the sample was safely in the nematic phase. Slowly cooling the liquid crystal through the isotropic–nematic phase transition ensures significant alignment of the director along the field direction. The magnetic coherence length at this field strength is $\sim 12\ \mu\text{m}$, much smaller than the sample dimensions. We illuminated the sample with ~ 10 mW of light at $\lambda = 514.5$ nm from an Ar-ion laser. For detection we used a multimode fiber coupled directly to a photomultiplier tube, from which the

detected photons were passed to a digital temporal autocorrelator with 25-ns minimum bin width.

Light is scattered in a liquid crystal by fluctuations of the local director. These fluctuations lead to a photon-scattering cross section that depends on the propagation direction of the incident and the scattered photons and on the directions of their electric polarization. The scattering cross section reaches a maximum for light traveling perpendicular to the director and vanishes to zero for light traveling parallel to the director. We expect this scattering anisotropy to cause the energy-density distribution in the steady state to be anisotropic. We intend to detect this anisotropy by measuring the diffuse transmission through the cell in directions parallel and perpendicular to the director, i.e., along the z and the y axes, re-
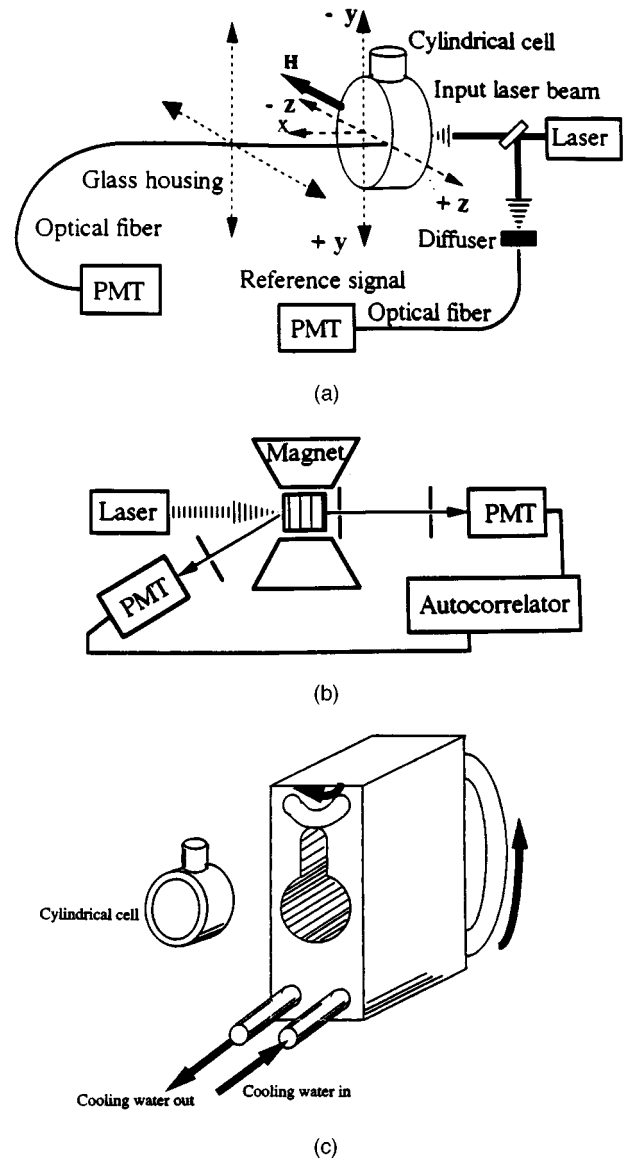

(a)

(b)

(c)

Fig. 4. (a) Diffuse transmission measurement. PMT, photomultiplier tube. (b) Temporal correlation measurement. The coordinate system chosen uses the x axis along the incident light direction, the z axis along the director, and the y axis along the direction perpendicular to both the director and the incident light direction. (c) Sample holder and cell.
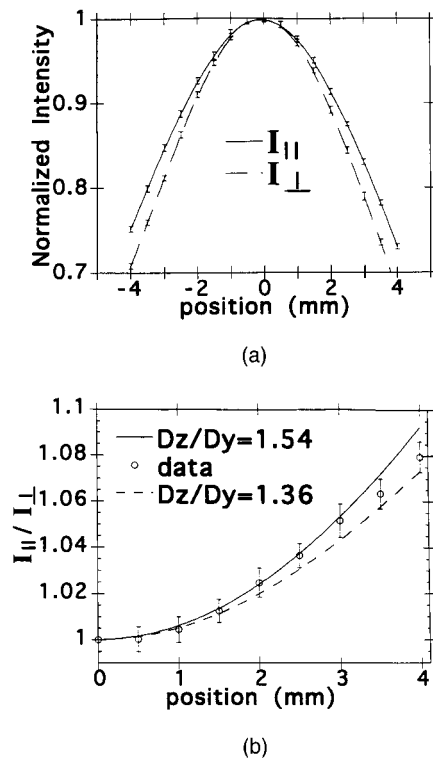
Fig. 5.   Anisotropic diffusive transmission in 5CB.   The coordinate system follows that given in Fig. 4.   (a) Normalized diffuse transmission intensity parallel and perpendicular to the director. (b) Ratio of the diffusive transmission intensity parallel to the director to that perpendicular to the director as a function of distance from the center of the cylindrical cell.   The dashed curve is the calculated result obtained by solution of Eq. (1.2.2).

spectively, in Fig. 4(a).   These results can be seen in Fig. 5.   The illuminating area of our input beam was ~1 mm^2. To minimize errors due to laser intensity fluctuations, we picked off a small amount of the input beam with a microscope slide placed in front of the sample and concurrently measured its transmission through a turbid colloidal suspension.   We normalized our nematic liquid-crystal transmission signal, using this weak reference beam.   The input beam direction was aligned perpendicular to the sample face and was approximately Gaussian.

Approximately 80% of the laser output was polarized perpendicular to the director.   With a combination of a polarizer and a half-wave plate, we were able to orient the polarization of the input beam so that it was mostly parallel or mostly perpendicular to the director.   We controlled the polarization of the detected light by placing a small piece of Polaroid over the tip of the detection fiber, which was attached to a $y–z$ translation stage.   The tip was located within 1 mm of the cell and was oriented perpendicular to the output cell face.   We translated the fiber parallel and perpendicular to the director and took relative intensity measurements (with respect to the reference signal) every 0.5 mm.   The average intensity measurements were made with the photon counter in our autocorrelator.   We counted at each position for 10 s, recording between 1 million and 10 million photons.

We first determined the center of the sample cell by finding the maximum transmitted intensity along both

the y and the z directions.   In particular, we made an initial scan along each axis.   We identified the center by assuming that the scan was symmetrical about the center, or maximum, and we located the midpoint between two positions of equal intensity about the center.   We did this for several different intensity pairs and then averaged these midpoints to find the center.   This process of determining the location of the center of the sample cell was accurate to approximately 0.1 mm.   Because of the opening in the sample cell (see Fig. 4), the boundary conditions at negative y are different from those at positive y.   As a result, we were forced to neglect the data far in the negative y direction.   After determining the center, we measured the transmitted intensity at each point, using four runs at each of the four possible input and output polarization combinations.   To within the error bars determined by the standard error in the average, all these runs exhibited the same transmission curve.   We therefore averaged over all 16 runs for our final analysis of the data. We determined the accuracy of the intensity measurements by finding, for each point, the standard deviation of the mean of each of the 16 runs performed.   This gave an accuracy of approximately 0.5%.

Clearly, there is anisotropy in transmission.   The relative widths of the transmission intensity profiles in directions parallel and perpendicular to the director establish that the $D_\parallel$ is larger than $D_\perp$.   In Fig. 5(a) we exhibit the transmitted intensity profile parallel to the director in both the positive and the negative z directions.   For the transmitted intensity profile perpendicular to the director, we consider only the positive y direction because of the asymmetry of the boundary conditions described above.   Also, a slight asymmetry about the center of the sample cell exists in the scan parallel to the director. This asymmetry is due, in part, to our not having located precisely the center of the sample cell and, therefore, the center of the intensity distribution.

In Fig. 5(b) we plot the ratio of parallel to perpendicular transmission as a function of radial position from the sample center.   The graph is an average of the positive z data and the negative z data, each divided by the data in the positive y direction.   The error equals the difference in each of these ratios.   This average takes into account the asymmetry in Fig. 5(a).   As expected, the anisotropy increases rapidly over the length scales probed.   By use of the anisotropic diffusion equation (1.2.8) for light transport applied in a cylindrical cell, it is possible to estimate the ratio of $D_\parallel$ to $D_\perp$.   The analytical solution to the isotropic diffusion equation for the cylindrical geometry is well known.   In the anisotropic case we expect the light to diffuse faster along the director than perpendicular to the director.   We can therefore apply the analytical isotropic solution to our problem by scaling the variable along the director (z) by the ratio of the diffusion constants, $D_\parallel/D_\perp$.   By fitting the data to the scaled analytical solution, we determine an optimum diffusion constant ratio.   To find the solution specific to our system, we also carefully considered the relatively small boundary-condition effects.   We estimated an extrapolation length[36] for the boundaries, i.e., a distance outside of the cell where the boundary can be considered to be completely absorbant, compensating for the reflected light at

the actual boundary. We took the extrapolations length z_0 to be βl^*, where $\beta = (1 + R)/(1 - R)$, with R being the reflectivity of our curved quartz surface. The l^* that we used was determined by comparison with a colloid, as described below. Because we scaled the axis along the director, we also scaled the extrapolation length along the director, by scaling β. This analysis yielded a best fit when the scaling factor was the ratio $D_\parallel/D_\perp = 1.60 \pm 0.25$.

In a set of control measurements, we filled the same cell with a colloidal suspension of polystyrene spheres of comparable optical density. The experiment was performed on this sample under identical circumstances, except that the magnetic field was turned off. These results can be seen in Fig. 6. Two important observations were made. First, no anisotropy in diffuse transmission was observed within the experimental error of 0.5%. This was expected, since there is no asymmetry in the structure of the colloid and, therefore, no asymmetry in the way that it scatters light. Second, by adjusting the particle concentration, we were able to achieve a transmission profile midway between the profiles shown in Fig. 5(a). From standard relations for colloids we then deduced a photon random-walk step length $l^* = 0.75 \pm 0.10$ mm for this concentration ($\phi = 0.003$) and particle diameter (204 nm). Then, using the relation $D = (c/n)l^*/3$, where n is the index of refraction of water, we obtained a value for the diffusion constant of the colloid of $D = 0.6 \times 10^9$ cm^2/s, which we identified with the average diffusion constant $(D_\parallel + D_\perp)/2$ of the nematic. From the measured ratio of the diffusion constants in the liquid crystal, $D_\parallel/D_\perp = 1.60 \pm 0.25$, we then estimated the absolute values of $D_\parallel = 0.7 \pm 0.1 \times 10^9$ cm^2/s and $D_\perp = 0.5 \pm 0.1 \times 10^9$ cm^2/s. This value for l^* also indicates that the sample thickness of 1 cm was more than 10 random-walk steps, confirming that light propagation was in the diffusing limit.

The dynamics of the system were probed in two different geometries. The measured temporal autocorrelation

Fig. 7. Dynamical temporal measurements in 5CB. (a) Forward scattering. (b) Backscattering.

functions for transmission and backscattering are shown in Fig. 7. For the transmission experiments, the input beam was aligned exactly as in the static experiment, i.e., normal to and in the center of the input cell face. We then measured the correlation function at two detector locations radially symmetric about the input beam (4 mm from the central axis), but with one detector displaced along the director and the other displaced perpendicular to the director. Because of the thickness of the sample, the count rate was low; therefore all the polarizers were eliminated from the setup to maximize the detected intensity. The rapid decay of the correlation function also decreased our count rate and required the use of our minimum bin width of 25 ns. With the laser aperture open and its output at 1.25 W, we had an average count rate of 50,000 counts/s. We performed four runs of the correlation experiment, each for 1 h. We then averaged these runs and determined error bars from the standard error of the average. We were able to obtain correlation functions in both cases, and, though we observed a slight difference within our signal-to-noise ratio as expressed in the error bars, it was difficult to distinguish between these two curves.

The setup for the backscattering experiment was quite different from those of the previous experiments. The input beam was ~4 mm in diameter, allowing us to analyze the system in an approximate plane-wave-in–point-out geometry. The output fiber detected backscattered light at an angle of ~14° at a distance of ~40 cm from the in-
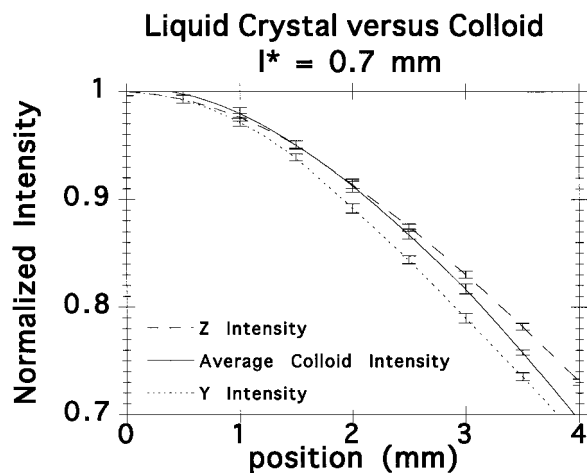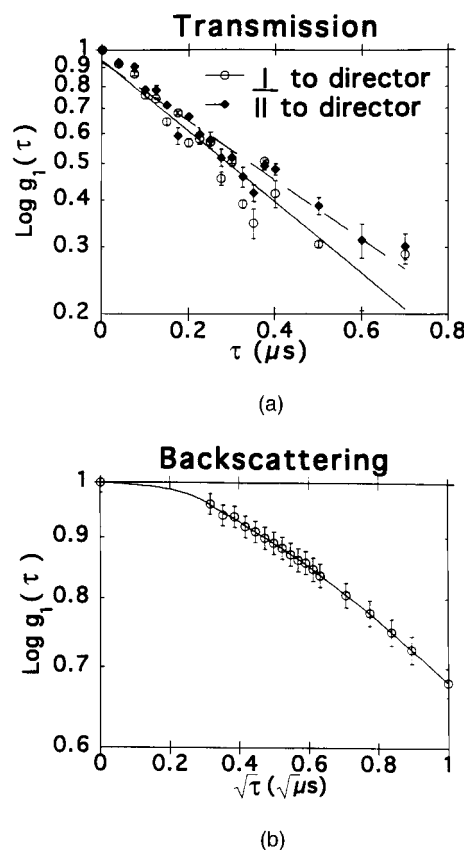

Fig. 6. Comparison of normalized diffuse transmission intensity of a colloid with the liquid-crystal transmission parallel and perpendicular to the director. The two colloid scans were averaged since they exhibited no anisotropy within our error; the colloid curve clearly falls between the liquid-crystal scans.

put face of the sample. The intensity detected in this geometry was greater than in transmission, so we were able to make polarization-dependent measurements, as we did for the intensity distribution case. With the laser output at 10 mW, we measured 10–40 kcnts/s. We took four measurements for each of the four polarization combinations and, seeing no significant difference in the different polarization measurements, we averaged all 16 of the runs as was done for the transmission experiment. Because of the finite size of the sample cell, the longest photon paths were cut off, causing a decrease in temporal decay of the correlation function. When analyzing the backscattering decay constant, we disregarded the early-time data, i.e., we fitted the long-time data.

To extract the temporal decay rates and hence the director's effective rotational viscosity, we used both the forward- and the backscattering normalized temporal correlation functions [Eq. (1.2.7)], $g_1(t)$, i.e.,

$$g_1(t) = \int_0^\infty \mathrm{d}T P(T) \exp[-(At/\gamma_{\mathrm{eff}})T], \qquad (1.3.1)$$

where $A = 2k_B T \Delta \epsilon^2 \omega^4 / 9\pi c^3 \sqrt{\epsilon_\perp}$ is a constant related to the optical anisotropy [relation (1.2.6)] and γ_{eff} is an effective viscosity, arising from an arithmetic and angular average of the mode viscosities.[28,29] We demanded that the light diffusion constants and the rotational viscosity agree in all the cases. By numerically generating solutions for each of the three geometries (two transmission and one backscattering) we obtained good agreement among the three values. The γ value was found to be 60 ± 10 cps, in reasonable agreement with the value of 70 cps that may be obtained by other techniques.[30,31] In addition, the average l^* value was found to be approximately 0.75 ± 0.2 mm.

2. THEORY OF MULTIPLE SCATTERING IN A NEMATIC

A. Properties of the Nematic Phase

Light scattering in the nematic phase occurs as a result of fluctuations in the local dielectric tensor $\epsilon_{ij}(\mathbf{r}, t)$, which in equilibrium is uniaxial with principal axis along the spatially uniform director $\mathbf{n}^0$. The dominant fluctuations in $\epsilon_{ij}(\mathbf{r}, t)$ arise from director fluctuations, and we can approximate $\epsilon_{ij}(\mathbf{r}, t)$ by a uniaxial tensor oriented along the local director $\mathbf{n}(\mathbf{r}, t)$:

$$\epsilon_{ij}(\mathbf{r}, t) = \epsilon_\perp \delta_{ij} + \Delta \epsilon n_i(\mathbf{r}, t) n_j(\mathbf{r}, t), \qquad (2.1.1)$$

where $\epsilon_\perp$ and $\epsilon_\parallel$ are the dielectric constants for electric fields, respectively, perpendicular and parallel to the director and $\Delta \epsilon = \epsilon_\parallel - \epsilon_\perp$ is the dielectric anisotropy. The energy cost arising from spatially nonuniform variation of $\mathbf{n}(\mathbf{r}, t)$ can be calculated from the Frank–Oseen–Zocher free energy[30,31]:

$$F[\mathbf{n}(\mathbf{r}, t)] = \frac{1}{2} \int [K_1(\nabla \cdot \mathbf{n})^2 + K_2(\mathbf{n} \cdot \nabla \times \mathbf{n})^2$$
$$+ K_3(\mathbf{n} \times \nabla \times \mathbf{n})^2 - \Delta \chi(\mathbf{n} \cdot \mathbf{H})^2] \mathrm{d}^3 r, \qquad (2.1.2)$$

where K_1, K_2, and K_3 are Frank elastic constants describing, respectively, the free energy associated with splay, twist, and bend distortions (see Fig. 8). We also include a magnetic-field term with $\Delta \chi = \chi_\parallel - \chi_\perp$ the anisotropy of the magnetic susceptibility. If $\Delta \chi > 0$, an alignment of the director parallel to the field $\mathbf{H}$ is favored. Even in a uniformly aligned sample there exist thermally induced fluctuations of the director,[37]

$$\mathbf{n}(\mathbf{r}, t) = \mathbf{n}^0 + \delta \mathbf{n}(\mathbf{r}, t), \qquad (2.1.3)$$

that lead to fluctuations in the local dielectric tensor and hence to scattering of light. This is the scattering process for which we want to formulate the theory of DWS. To do so, we have to consider light propagation in a homogeneous uniaxial medium (Subsection 2.B). Then we consider the fluctuations in the dielectric tensor (see Subsection 2.C) to understand single-scattering processes. Finally, we investigate multiple-scattering events (Subsections 2.D and 2.E) and report on numerical simulations (Subsection 2.F).

B. Light Propagation in a Homogeneous Nematic

In this section we review light propagation in uniaxial media and rederive familiar expressions[34,35,38] for the phase and the group velocities of the ordinary and the extraordinary waves.

A nematic liquid crystal is a uniaxial medium in which light propagates in ordinary and extraordinary rays with different polarizations and speeds of light. The ordinary ray has a polarization that is perpendicular to both the wave vector $\mathbf{k}$ and the equilibrium director $\mathbf{n}^0$. Its phase and group velocities are parallel to $\mathbf{k}$, with magnitudes independent of the direction of $\mathbf{k}$. The extraordinary ray has a polarization in the $\mathbf{k}$–$\mathbf{n}^0$ plane. Its phase and group velocities are not parallel, and their magnitudes depend on the wave vector $\mathbf{k}$, which is parallel to the phase velocity. Figure 9 summarizes the geometry for light propagation. $\hat{\mathbf{u}}_1$ and $\hat{\mathbf{u}}_2$ are orthogonal unit vectors perpendicular to $\mathbf{n}^0$. $\hat{\mathbf{u}}_1$ lies in the $\mathbf{k}$–$\mathbf{n}^0$ plane, and $\hat{\mathbf{u}}_2$ is perpendicular to this plane. The wave vector $\mathbf{k}$ makes an angle θ with $\mathbf{n}^0$. For the ordinary ray, the electric field $\mathbf{E}$
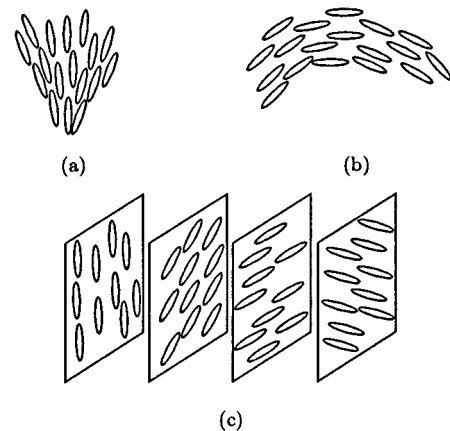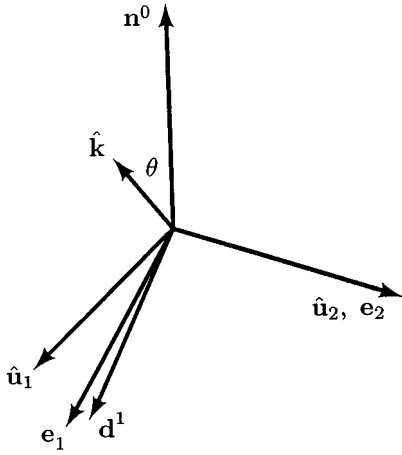

Fig. 8. Pure splay, twist, and bend modes.

Fig. 9.   Directions of polarization vectors $\mathbf{e}_1$, $\mathbf{d}^1$ and $\mathbf{e}_2$, $\mathbf{d}^2$ in relation to Frank director $\mathbf{n}_0$ and to wave vectors $\mathbf{k}$, $\hat{\mathbf{u}}_1$, and $\hat{\mathbf{u}}_2$. Vectors $\mathbf{n}_0$, $\hat{\mathbf{u}}_1$, and $\hat{\mathbf{u}}_2$ also form the basis for describing director fluctuations of wave vector $\mathbf{k}$.

and the displacement $\mathbf{D}$ are parallel to $\hat{\mathbf{u}}_2$. For the extraordinary ray, the displacement vector $\mathbf{D}$ is parallel to $-\cos\theta\mathbf{n}^0 + \sin\theta\hat{\mathbf{u}}_1$.

Light propagation is determined by the Maxwell wave equation

$$[(\nabla^2\delta_{ij} - \nabla_i\nabla_j) - (\partial^2/\partial t^2)\epsilon_{ij}(\mathbf{r}, t)]E_j(\mathbf{r}, t) = 0. \tag{2.2.1}$$

To discuss light propagation in a homogeneous nematic, we ignore fluctuations of the dielectric tensor and use Eq. (2.1.1) with the equilibrium Frank director $\mathbf{n}^0$:

$$\epsilon_{ij}^0 = \epsilon_\perp\delta_{ij} + \Delta\epsilon n_i^0 n_j^0. \tag{2.2.2}$$

The dielectric displacement $\mathbf{D}$ and the electric field $\mathbf{E}$ are related in the usual way:

$$D_i = \epsilon_{ij}^0 E_j. \tag{2.2.3}$$

In the absence of free charge, the divergence of $\mathbf{D}$ is zero:

$$\nabla_i D_i = \nabla_i \epsilon_{ij}^0 E_j = 0. \tag{2.2.4}$$

With the plane-wave ansatz for the electric field:

$$\mathbf{E}(\mathbf{r}, t) = E^\alpha\mathbf{e}_\alpha(\hat{\mathbf{k}})\exp[i(\mathbf{k}\cdot\mathbf{r} - \omega t)], \tag{2.2.5}$$

we transform the wave equation (2.2.1) to a generalized eigenvalue equation:

$$[k^2(\delta_{ij} - \hat{k}_i\hat{k}_j) - (\omega^2/c^2)\epsilon_{ij}^0]e_{\alpha j}(\hat{\mathbf{k}}) = 0, \tag{2.2.6}$$

which determines the electric-polarization vector $\mathbf{e}_\alpha(\hat{\mathbf{k}})$ and a direction-dependent index of refraction

$$n_\alpha(\hat{\mathbf{k}}) = ck/\omega \tag{2.2.7}$$

for the two possible electric-field modes.

We now construct basis vectors $\mathbf{e}_\alpha$ for the electric field and $\mathbf{d}^\alpha$ for the displacement field.[29,38] These vectors are depicted in Fig. 9. We begin by defining $\mathbf{d}^\alpha(\hat{\mathbf{k}})$ for the dielectric displacement through

$$d_i^\alpha = \epsilon_{ij}^0 e_{\alpha j}. \tag{2.2.8}$$

Because $\mathbf{D} = d^\alpha D_\alpha \exp[i(\mathbf{k}\cdot\mathbf{r} - \omega t)]$ is transverse, $\mathbf{k}\cdot\mathbf{d}^\alpha = 0$. Equation (2.2.6) can then be used to show that the vectors $\mathbf{e}_\alpha(\mathbf{k})$ are perpendicular to $\epsilon_{ij}^0 k_j$ and that $\mathbf{e}_\alpha$ and $\mathbf{d}^\alpha$ are dual to each other so that their magnitudes can be chosen to satisfy the biorthogonality relation

$$\mathbf{d}^\alpha \cdot \mathbf{e}_\beta = \delta_\beta^\alpha. \tag{2.2.9}$$

For the ordinary ray, $\mathbf{d}^2$ is parallel to $\hat{\mathbf{u}}_2$, and $e_{2i} = (\epsilon^0)_{ij}^{-1} d_j^2$. Thus, to satisfy Eq. (2.2.9), we chose

$$\mathbf{e}_2 = \frac{1}{n_2}\hat{\mathbf{u}}_2, \quad \mathbf{d}^2 = n_2\hat{\mathbf{u}}_2, \tag{2.2.10}$$

where the unit vector $\hat{\mathbf{u}}_2$ is perpendicular to both the Frank director $\mathbf{n}^0$ and the wave vector $\mathbf{k}$, which enclose the angle θ, and where n_2 is the refractive index of the ordinary ray, satisfying

$$\frac{1}{n_2^2} = \frac{1}{\epsilon_\perp}. \tag{2.2.11}$$

Now we can construct the polarization vectors of the extraordinary light wave. From the biorthogonality condition (2.2.9) it follows that they lie in the plane spanned by $\mathbf{n}^0$ and $\mathbf{k}$. In addition, the polarization vector $\mathbf{d}^1$ has to be perpendicular to $\mathbf{k}$:

$$\mathbf{d}^1 = n_1(\hat{\mathbf{k}})(-\sin\theta\,\mathbf{n}^0 + \cos\theta\,\hat{\mathbf{u}}_1), \tag{2.2.12}$$

where the unit vector $\hat{\mathbf{u}}_1$ is perpendicular to $\mathbf{n}^0$. Then we obtain $\mathbf{e}_1$ from $e_{1i} = \epsilon_{ij}^{0-1} d_j^1$:

$$\mathbf{e}_1 = n_1\left(-\frac{\sin\theta}{\epsilon_\parallel}\mathbf{n}^0 + \frac{\cos\theta}{\epsilon_\perp}\hat{\mathbf{u}}_1\right). \tag{2.2.13}$$

The normalization of $\mathbf{d}^1$ and $\mathbf{e}_1$ is determined by Eq. (2.2.9), and the refraction index $n_1(\hat{\mathbf{k}})$ is identified with the help of the eigenvalue equation (2.2.6):

$$\frac{1}{n_1^2(\hat{\mathbf{k}})} = \frac{\sin^2\theta}{\epsilon_\parallel} + \frac{\cos^2\theta}{\epsilon_\perp}. \tag{2.2.14}$$

The angle δ_1 between $\mathbf{e}_1$ and $\mathbf{d}^1$ satisfies

$$\cos\delta_1 = \frac{1}{n_1^2(\hat{\mathbf{k}})}\left(\frac{\sin^2\theta}{\epsilon_\parallel^2} + \frac{\cos^2\theta}{\epsilon_\perp^2}\right)^{-1/2}. \tag{2.2.15}$$

For the ordinary light wave $\delta_2 = 0$. Finally, we note that the projection operator $\delta_{ij} - \hat{k}_i\hat{k}_j$ can conveniently be written as

$$\delta_{ij} - \hat{k}_i\hat{k}_j = \sum_\alpha \frac{1}{n_\alpha^2} d_i^\alpha d_j^\alpha. \tag{2.2.16}$$

It is important to remember, especially when comparing with formulas for isotropic systems, that neither $\mathbf{d}^\alpha$ nor $\mathbf{e}_\alpha$ is a unit vector: $\mathbf{d}^\alpha$ has magnitude n_α, whereas $\mathbf{e}_\alpha$ has a magnitude that scales as an inverse index of refraction. In addition, E_α is really $\sqrt{4\pi}$ times an energy density rather than an electric field. This follows because $\mathbf{E}\cdot\mathbf{D} = \Sigma_\alpha E_\alpha^2$ and $\mathbf{E}\cdot\mathbf{D}/4\pi$ is the energy density.

There are two velocities, the phase and the group velocities, associated with wave propagation. We need to discuss them in more detail. Light modes are characterized by the dispersion relation

$$\omega_\alpha{}^2(\mathbf{k}) = \frac{c^2 k^2}{n_\alpha{}^2(\hat{\mathbf{k}})} = v_{p\alpha}{}^2(\hat{k}) k^2, \qquad (2.2.17)$$

for each polarization α, where $v_{p\alpha}(\hat{\mathbf{k}}) = c/n_a(\hat{\mathbf{k}})$ is the phase velocity, which depends on direction for the extraordinary ray. Equivalently, modes can be characterized by the wave vectors

$$\mathbf{k}^\alpha = n_\alpha(\hat{\mathbf{k}}) \frac{\omega}{c} \hat{\mathbf{k}} \equiv \frac{\omega}{v_{p\alpha}(\hat{\mathbf{k}})} \hat{\mathbf{k}}. \qquad (2.2.18)$$

For a given frequency ω, the wave vector $\mathbf{k}^\alpha$ lies on the wave-vector surface, which, as shown in Fig. 10, is a circle of radius $n_2 \omega/c$ for the ordinary ray ($\alpha = 2$) and an ellipse with semiaxes $\sqrt{\epsilon_\perp}\,\omega/c$ and $\sqrt{e_\parallel}\,\omega/c$ for the extraordinary light wave ($\alpha = 1$). In numerical simulations, on which we report below, we follow the paths of single photons. They transport energy and thus propagate along the Poynting vector, which is given by the energy density of the light wave times the group velocity $\mathbf{v}_{g\alpha} = \nabla_{\mathbf{k}}\omega_\alpha(\mathbf{k})$.[34] For the ordinary ray $\mathbf{v}_{g2} = \mathbf{v}_{p2} \parallel \hat{\mathbf{k}}^2$. The group velocity of the extraordinary wave:

$$\mathbf{v}_{g1}(\hat{\mathbf{k}}) = \frac{1}{2\omega_1(\mathbf{k})} \nabla_{\mathbf{k}}\omega_1{}^2(\mathbf{k}) \equiv v_{g1}\mathbf{e}_{g1}(\hat{\mathbf{k}})$$

$$= \frac{c n_1(\hat{\mathbf{k}})}{k} \left(\frac{k_\parallel}{\epsilon_\perp} \mathbf{n}^0 + \frac{k_\perp}{\epsilon_\parallel} \hat{\mathbf{u}}_1 \right). \qquad (2.2.19)$$

is normal to the wave-vector surface, as illustrated in Fig. 10. The unit vector $\mathbf{e}_{g1}(\hat{\mathbf{k}})$ is parallel to $\mathbf{v}_{g1}(\hat{\mathbf{k}})$ and normal to the wave-vector surface. The phase velocity makes an angle θ_R with the director $\mathbf{n}^0$ given by

$$\cos\theta_R = \frac{n_1{}^2(\hat{\mathbf{k}})}{\epsilon_\perp} \cos\delta_1 \cos\theta, \qquad (2.2.20)$$

where δ_1 denotes the angle between the polarization vectors $\mathbf{e}_1$ and $\mathbf{d}^1$, which we introduced in Eq. (2.2.15). δ_1 is also the angle between $\hat{\mathbf{k}} \parallel \mathbf{v}_{p1}$ and $\mathbf{v}_{g1}$, implying the relation

$$v_{g1} \cos\delta_1 = \mathbf{v}_{g1} \cdot \hat{\mathbf{k}} = v_{p1} = c/n_1(\hat{\mathbf{k}}) \qquad (2.2.21)$$
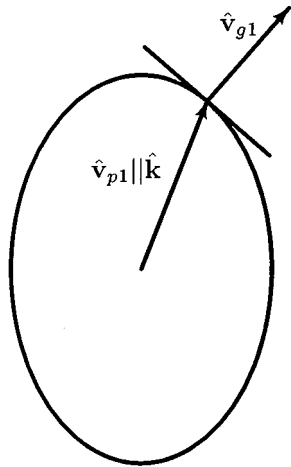

Fig. 10.   Diagram showing the wave-vector surface and the directions of the phase and the group velocities.

between the magnitudes of the group and the phase velocities. Finally, we note that the Poynting vector for polarization α,

$$\mathbf{S}_\alpha = [1/(4\pi)] E_\alpha{}^2 \mathbf{v}_{g\alpha}, \qquad (2.2.22)$$

is the group velocity times the energy density. This can be derived by use of Maxwell's equations and the relations between phase and group velocity reviewed in this section.

C.   Fluctuations of the Director and the Dielectric Tensor

We now allow the director to fluctuate around its equilibrium value: $\mathbf{n}(\mathbf{r}, t) = \mathbf{n}^0 + \delta\mathbf{n}(\mathbf{r}, t)$. For small fluctuations we have $\delta\mathbf{n}(\mathbf{r}, t) \perp \mathbf{n}^0$ since $\mathbf{n}(\mathbf{r}, t)$ is a unit vector. We write the Fourier transform $\delta\mathbf{n}(\mathbf{q}, t) = \int d^3 r\, \delta\mathbf{n}(\mathbf{r}, t) \exp i\mathbf{q} \cdot \mathbf{r}$ in the basis shown in Fig. 9:

$$\delta\mathbf{n}(\mathbf{q}, t) = \delta n_1(\mathbf{q}, t)\hat{\mathbf{u}}_1 + \delta n_2(\mathbf{q}, t)\hat{\mathbf{u}}_2, \quad (2.3.1)$$

where the amplitudes $\delta n_\delta(\mathbf{q}, t)$ ($\delta = 1, 2$) characterize the different director modes. Then the Frank free energy, Eq. (2.1.2), takes the form

$$F[\mathbf{n}(\mathbf{r}, 0)] = \frac{1}{2} \sum_{\delta=1}^{2} \int \frac{d^3 q}{(2\pi)^3} K_\delta(\mathbf{q}) |\delta n_\delta(\mathbf{q}, 0)|^2, \qquad (2.3.2)$$

with $\mathbf{q}$-dependent elastic constants

$$K_\delta(\mathbf{q}) = K_\delta q_\perp{}^2 + K_3 q_\parallel{}^2 + \Delta\chi H^2, \qquad (2.3.3)$$

where $q_\perp$ and $q_\parallel$ are, respectively, the components of $\mathbf{q}$ perpendicular and parallel to $\mathbf{n}^0$. If we choose $q_\parallel = 0$, the director modes are pure splay ($\delta = 1$) or twist ($\delta = 2$) modes. For $q_\perp = 0$, we obtain two bend modes. The distortions corresponding to these modes are illustrated in Fig. 8. For a general wave vector $\mathbf{q}$, the modes contain a combination of bend and either splay or twist deformations.

Quasi-elastic light-scattering experiments in nematics measure the time-dependent director autocorrelation function[30,31,39]

$$\langle \delta n_\delta(\mathbf{q}, t) \delta n_\delta^*(\mathbf{q}, 0) \rangle = \frac{k_B T}{K_\delta(\mathbf{q})} \exp\left[-\frac{K_\delta(\mathbf{q})}{\eta_\delta(\mathbf{q})} t \right]. \qquad (2.3.4)$$

The first factor in this expression results from the application of the equipartition theorem, which states that each director mode has an average thermal energy $k_B T/2$. The second factor reflects the purely diffusive temporal decay of the director modes. The relaxation frequency is given by the quotient of elastic, $K_\delta(\mathbf{q})$, and viscous, $\eta_\delta(\mathbf{q})$, forces. To arrive at this result, one has to analyze the Leslie–Erickson equations.[30,31,40] They comprise the Navier–Stokes equations for a uniaxial medium, which describe the fluid motion, and dynamical equations for the director. The viscosity $\eta_\delta(\mathbf{q})$ is a combination of several Leslie viscosities that appear in these equations. The important contribution to $\eta_\delta(\mathbf{q})$ comes from the rotational viscosity γ, which measures viscous forces hindering the rotation of the director. In Eq. (2.3.4) we have neglected a second fast mode, whose character is

predominantly that of velocity diffusion. Its characteristic frequency $(\eta/\rho)q^2$ (where $\rho \approx 1$ gm/cm^3 is the mass density) is much greater than $\Gamma_{\mathbf{q}}$, since $\eta\rho \sim 10^{-1}$ cm^2/s is much greater than $K/\eta \sim 10^{-5}$–10^{-6} cm^2/s.

The spatial autocorrelation functions $\langle \delta n_\delta(\mathbf{R}, 0) \times \delta n_\delta(\mathbf{0}, 0) \rangle$, where $\delta = 1, 2$ stands for the two components perpendicular to $\mathbf{n}^0$, follow from Eq. (2.3.4) after a Fourier transformation. In the one-constant approximation $(K = K_i)$ it reads[30]

$$\langle \delta n_\delta(\mathbf{R}, 0)\delta n_\delta(\mathbf{0}, 0) \rangle \propto (1/R)\exp(-R/\xi), \quad (2.3.5)$$

where the magnetic coherence length

$$\xi = \sqrt{\frac{K}{\Delta\chi H^2}} \qquad (2.3.6)$$

gives the length scale over which director fluctuations are correlated.

The director fluctuations induce fluctuations $\delta\epsilon_{ij}(\mathbf{r}, t)$ of the dielectric tensor. They follow from Eq. (2.1.1) to first order in $\delta\mathbf{n}(\mathbf{r}, t)$:

$$\delta\epsilon_{ij}(\mathbf{r}, t) = \Delta\epsilon[\delta n_i(\mathbf{r}, t)n_j{}^0 + n_i{}^0\delta n_j(\mathbf{r}, t)]. \qquad (2.3.7)$$

The scattered electric field for a single-light-scattering event is proportional to the Fourier component

$$\delta\epsilon_{\alpha\beta}(\mathbf{k}^\alpha - \mathbf{q}^\beta, t) = e_{\alpha i}\delta\epsilon_{ij}(\mathbf{k}^\alpha - \mathbf{q}^\beta, t)e_{\beta j}, \qquad (2.3.8)$$

where the pairs $\mathbf{k}^\beta$, $\mathbf{e}_\beta$ and $\mathbf{k}^\alpha$, $\mathbf{e}_\alpha$ stand, respectively, for the wave vector and the polarization of the incoming and the scattered electric field. In experiments one measures the temporal autocorrelation function of the scattered electric field through time correlations in the light intensity. For single scattering this autocorrelation function is proportional to

$$B_{\alpha\beta}(\hat{\mathbf{k}}, \hat{\mathbf{q}}, t) = (\omega^4/c^4)\langle \delta\epsilon_{\alpha\beta}(\mathbf{k}^\alpha - \mathbf{q}^\beta, t)$$
$$\times \; \delta\epsilon_{\alpha\beta}{}^*(\mathbf{k}^\alpha - \mathbf{q}^\beta, 0)\rangle, \qquad (2.3.9)$$

where ω is the angular frequency of light. We call $B_{\alpha\beta}(\hat{\mathbf{k}}, \hat{\mathbf{q}}, t)$ a structure factor because it contains information about the elastic and the dynamic properties of the director modes. Using $\delta\epsilon_{ij}(\mathbf{r}, t)$ from Eq. (2.3.7) and the autocorrelation function of Eq. (2.3.4), we obtain

$$B_{\alpha\beta}(\hat{\mathbf{k}}, \hat{\mathbf{q}}, t)$$
$$= (\Delta\epsilon)^2 k_B T \frac{\omega^4}{c^4} \sum_{\delta=1}^{2} \frac{N(\mathbf{e}_\alpha, \mathbf{e}_\beta, \hat{\mathbf{u}}_\delta)}{K_\delta(\mathbf{q}_s)} \exp\left[-\frac{K_\delta(\mathbf{q}_s)}{\eta_\delta(\mathbf{q}_s)}t\right], \qquad (2.3.10)$$

with

$$\mathbf{q}_s = (\omega/c)(n_\alpha\hat{\mathbf{k}}_\alpha - n_\beta\hat{\mathbf{q}}_\beta) \qquad (2.3.11)$$

and with

$$N(\mathbf{e}_\alpha, \mathbf{e}_\beta, \hat{\mathbf{u}}_\delta) = [(\mathbf{n}^0 \cdot \mathbf{e}_\beta)(\hat{\mathbf{u}}_\delta \cdot \mathbf{e}_\alpha)$$
$$+ (\hat{\mathbf{u}}_\delta \cdot \mathbf{e}_\beta)(\mathbf{n}^0 \cdot \mathbf{e}_\alpha)]^2, \qquad (2.3.12)$$

a geometry factor. Note that $N(\mathbf{e}_\alpha, \mathbf{e}_\beta, \hat{\mathbf{u}}_\delta)$ is zero if both $\mathbf{e}_\alpha$ and $\mathbf{e}_\beta$ are perpendicular to $\mathbf{n}^0$. This means that there is no director-induced ordinary-to-ordinary scattering.

There is only scattering from an ordinary ray to an extraordinary ray and vice versa, and scattering from an extraordinary ray to an extraordinary ray. Of course, there is ordinary-to-ordinary scattering produced by fluctuations in the isotropic part of the dielectric tensor. This, however, is much smaller than the director-induced scattering, and we ignore it.

The structure factor is related to the differential cross section giving the scattered energy per unit of time, solid angle element, and incident intensity in a medium of volume V:[41]

$$\frac{d\sigma^{\alpha\beta}}{d\Omega_k{}^\alpha} = \frac{V}{(4\pi)^2}\,n_\alpha{}^3(\hat{\mathbf{k}})B_{\alpha\beta}(\hat{\mathbf{k}}, \hat{\mathbf{q}}, t = 0)n_\beta(\hat{\mathbf{q}})\cos\,\delta_\beta. \qquad (2.3.13)$$

The indices α and β denote, respectively, the modes of the scattered and the incident light. Note that here we use the solid angle element $d\Omega_k{}^\alpha$ for the wave vector. For extraordinary light, it differs from the solid angle element $d\Omega_R{}^\alpha$ of the Poynting vector, which is relevant for experiment. The connection between the two is given by

$$\frac{d\Omega_R{}^1}{d\Omega_k{}^1} = \frac{d\cos\theta_R}{d\cos\theta} = \frac{n_1{}^6(\hat{\mathbf{k}})\cos^3\delta_1}{\epsilon_\perp{}^2\epsilon_\parallel}, \qquad (2.3.14)$$

where we used Eqs. (2.2.20) and (2.2.14). In comparing Eqs. (2.3.9) and (2.3.10) with results for isotropic systems, it is useful to recall how quantities scale with dielectric constant or index of refraction. Normally one would expect $\delta\epsilon_{\alpha\beta}$ to scale as a dielectric constant. However, because of the normalization of $\mathbf{e}_\alpha$, $\delta\epsilon_{\alpha\beta}$ has no scale. The cross section, in contrast, scales as $B_{\alpha\beta}$ times an index of refraction to the fourth power, i.e., it scales as the square of a dielectric constant, as it does in an isotropic system.

D. Fluctuations in ϵ_{ij} and Damping

Fluctuations in density, the Frank director, and other quantities, give rise to fluctuations $\delta\epsilon_{ij}(\mathbf{r}, t)$ in the local dielectric constant from its equilibrium value $\epsilon_{ij}{}^0$:

$$\epsilon_{ij}(\mathbf{r}, t) = \epsilon_{ij}{}^0 + \delta\epsilon_{ij}(\mathbf{r}, t). \qquad (2.4.1)$$

Fluctuations in ϵ_{ij} lead to fluctuations in the local plane-wave amplitudes. To describe this situation, we assume that the frequency of input radiation is ω, and we decompose $\mathbf{E}(\mathbf{r}, t)$ into polarization components determined by $\mathbf{e}_\alpha$:

$$\mathbf{E}(\mathbf{r}, t) = \mathbf{e}_\alpha(\hat{\nabla})E^\alpha(\mathbf{r}, t)\exp(-i\omega t), \qquad (2.4.2)$$

where $\hat{\nabla} = \nabla/|\nabla|$. The frequencies of temporal variations of $\mathbf{E}^\alpha(\mathbf{r}, t)$ are determined by those of $\delta\epsilon_{ij}$, which are slow compared with the light frequency ω. In this limit we can use the slowly varying amplitude approximation in which the frequency of temporal variation of the amplitude $E^\alpha(\mathbf{r}, t)$ is much slower than ω. Then $\partial^2/\partial t^2\epsilon_{ij}(\mathbf{r}, t)E_j(\mathbf{r}, t) = -(\omega^2/c^2)\epsilon_{ij}(\mathbf{r}, t)E_j(\mathbf{r}, t)$. Taking the dot product of Eq. (2.2.1) with $e_{\alpha i}$ and using Eqs. (2.2.9) and (2.2.16), we obtain

$$\left[-\frac{1}{n_\alpha{}^2(\hat{\nabla})}\nabla^2 - \frac{\omega^2}{c^2}\right]E_\alpha(\mathbf{r}, t) = \frac{\omega^2}{c^2}\delta\epsilon_{\alpha\beta}(\mathbf{r}, t)E_\beta(\mathbf{r}, t), \qquad (2.4.3)$$

where

$$\delta\epsilon_{\alpha\beta}(\mathbf{r},\,t) = \mathbf{e}_i{}^\alpha(\hat{\nabla})\delta\epsilon_{ij}(\mathbf{r},\,t)\mathbf{e}_j{}^\beta(\hat{\nabla}). \qquad (2.4.4)$$

Note that $\delta\epsilon_{\alpha\beta}(\mathbf{r},\,t)$ is actually an operator because of the gradient dependence of the polarization vectors. The order of these vectors is important: the gradient in the left vector acts on all that follows it, including $\delta\epsilon_{ij}(\mathbf{r},\,t)$.

Equation (2.4.3) is now in a standard form for the application of diagrammatic perturbation theory.[29,42,43] Appendix A outlines the calculation of the average Green function, $G_\alpha(\mathbf{k},\,\omega)$, for propagation of light with polarization α in the weak-scattering limit from the graphs shown in Fig. 11. The result is

$$G_\alpha{}^{-1}(\mathbf{k},\,\omega) = \frac{k^2}{n_\alpha{}^2(\hat{\mathbf{k}})} - \frac{\omega^2}{c^2} - \frac{i\omega}{c}\frac{1}{n_\alpha(\hat{\mathbf{k}})l_\alpha(\hat{\mathbf{k}},\,\omega)}, \qquad (2.4.5)$$

where the bare mean free path $l_\alpha(\hat{\mathbf{k}},\,\omega)$ is determined by[44]

$$\frac{4\pi}{l_\alpha(\hat{\mathbf{k}},\,\omega)} = n_\alpha(\hat{\mathbf{k}})\sum_\beta \int \frac{\mathrm{d}\Omega_q}{4\pi} B_{\alpha\beta}(\hat{\mathbf{k}},\,\hat{\mathbf{q}},\,t=0)n_\beta{}^3(\hat{\mathbf{q}}), \qquad (2.4.6)$$

where $B_{\alpha,\beta}(\hat{\mathbf{k}},\,\hat{\mathbf{q}},\,t)$ is defined in Eq. (2.3.9) and $\mathbf{k}^\alpha$ is given by Eq. (2.2.18). The physical mean free path l'_α, as we show below, is equal to $l_\alpha/\cos\delta_\alpha$.

We show in Appendix A that Eq. (2.4.6) implies that the mean free path for extraordinary-to-extraordinary scattering tends to zero as $(\ln\Delta\chi H^2)^{-1}$ as $H\to 0$. This would seem to invalidate the approximations of the weak-scattering limit. However, scattering in this limit is highly peaked in the forward-scattering direction so that it takes many scattering events to change the direction of light propagation. Thus, as we show below, the transport mean free paths, and thus the photon diffusion constants, are perfectly finite.

To discuss multiple scattering in real space, we need the spatial Fourier transform of $G_\alpha(\mathbf{k},\,\omega)$. The Green function for the ordinary ray is isotropic and identical in form to that of an isotropic medium:

$$G_2(\mathbf{R},\,\omega) = \frac{n_2{}^3}{4\pi n_2 R}\exp[in_2(\omega/c)R]\exp(-R/2l_2). \qquad (2.4.7)$$

The Green function for the extraordinary wave is more complicated,[38] but it can be calculated straightforwardly by anisotropic rescaling of lengths and wave vectors in
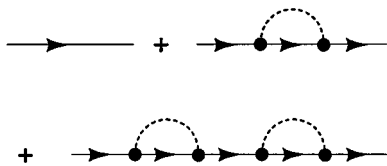

Fig. 11. Graphs for the photon Green function in the weak-scattering limit.

$$G_1(\mathbf{r},\,\omega) = \int \frac{\mathrm{d}^3k}{(2\pi)^3}\exp(i\mathbf{k}\cdot\mathbf{R})\left[\frac{k_\|{}^2}{\epsilon_\perp} + \frac{k_\perp{}^2}{\epsilon_\|} - \frac{\omega^2}{c^2}\right.$$
$$\left. - i\frac{\omega}{c}\frac{1}{n_1(\hat{\mathbf{k}})l_1(\hat{\mathbf{k}},\,\omega)}\right]^{-1}$$
$$= \frac{\epsilon_\|\sqrt{\epsilon_\perp}}{4\pi R'}\exp[i(\omega/c)R']\exp[-R'/(2l_1)], \qquad (2.4.8)$$

where

$$\mathbf{R}' = \sqrt{\epsilon_\|}\mathbf{R}_\perp + \sqrt{\epsilon_\perp}\mathbf{R}_\|. \qquad (2.4.9)$$

The Green function gives the electric field at $\mathbf{R}$ in response to a disturbance at the origin. Thus $\mathbf{R}$ is parallel to the group velocity $\mathbf{v}_{g1}(\hat{\mathbf{R}})$, where $\hat{\mathbf{R}}$ is the unit vector parallel to $\mathbf{R}$. The wave vector $\mathbf{k}_R{}^1$ that produces a group velocity parallel to $\mathbf{R}$ must, from Eq. (2.2.19), have the form $\mathbf{k}_R{}^1 = A(\epsilon_\perp\mathbf{R}_\| + \epsilon_\|\mathbf{R}_\perp)$, where A is determined by the requirement that $(k_R{}^1)^2/n_1{}^2(\hat{\mathbf{k}}_R{}^1) = (\omega/c)^2$. These considerations imply that

$$\mathbf{k}_R{}^1 = \frac{\omega}{c}\frac{\epsilon_\perp\mathbf{R}_\| + \epsilon_\|\mathbf{R}_\perp}{\sqrt{\epsilon_\perp R_\|{}^2 + \epsilon_\| R_\perp{}^2}} = \frac{\omega}{c}n_1(\hat{\mathbf{k}}_R{}^1)\hat{\mathbf{k}}_R{}^1, \qquad (2.4.10)$$

$$\frac{\omega}{c}R' = \mathbf{k}_R{}^1\cdot\mathbf{R} = \frac{\omega n_1(\hat{\mathbf{k}}_R{}^1)}{c}R\cos\delta_1, \qquad (2.4.11)$$

and $R' = n_1 R\cos\delta_1$. Thus the Green function for the extraordinary ray can be rewritten as

$$G_1(\mathbf{R},\,\omega) = \frac{\epsilon_\|\sqrt{\epsilon_\perp}}{4\pi n_1 R\cos\delta_1}\exp(i\mathbf{k_R}{}^1\cdot\mathbf{R})$$
$$\times \exp(-R\cos\delta_1/2l_1). \qquad (2.4.12)$$

From this we see that the physical mean free path for extraordinary photons is

$$l_1' = \frac{l_1}{\cos\delta_1}. \qquad (2.4.13)$$

rather than l_1.

E. Multiple Scattering and Diffusion
In this section, we consider multiple scattering in a nematic liquid crystal and show how it leads to energy diffusion with anisotropic diffusion coefficients. The intensity of radiation measured at the detector can be obtained from the function

$$\mathscr{G}_\alpha(\mathbf{R},\,\mathbf{r},\,T,\,t) = \left\langle E^\alpha\!\left(\mathbf{R} + \frac{\mathbf{r}}{2},\,T + \frac{t}{2}\right)\right.$$
$$\left. \times E^{\alpha*}\!\left(\mathbf{R} - \frac{\mathbf{r}}{2},\,T - \frac{t}{2}\right)\right\rangle, \qquad (2.5.1)$$

which is determined by the source intensity $J_\alpha(\mathbf{R}',\,\mathbf{r}',\,T')$ and the energy propagator $\Phi^{\alpha\beta}(\mathbf{R} - \mathbf{R}',\,\mathbf{r},\,\mathbf{r}',\,T - T',\,t)$ through

$$\mathscr{G}_\alpha(\mathbf{R},\,\mathbf{r},\,T,\,t) = \int \mathrm{d}^3R'\mathrm{d}^3r'\mathrm{d}T'\Phi^{\alpha\beta}(\mathbf{R}-\mathbf{R}',\,\mathbf{r},\,\mathbf{r}',$$
$$\times\, T - T',\, t)J_\beta(\mathbf{R}',\,\mathbf{r}',\,T',\,t).$$

$$(2.5.2)$$

In the weak-scattering diffusion approximation, $\Phi^{\alpha\beta}$ can be expressed as a sum of ladder diagrams,[29,42,43] as shown in Fig. 12, which reduce in Fourier space to the Bethe–Salpeter equation

$$\Phi_{\mathbf{k},\mathbf{k}'}{}^{\alpha\beta}(\mathbf{K},\,\Omega,\,t) = \delta^{\alpha\beta}f_\mathbf{k}{}^\alpha(\mathbf{K},\,\Omega)(2\pi)^2\delta(\mathbf{k}-\mathbf{k}')$$

$$+ \int \frac{\mathrm{d}^3k_1}{(2\pi)^3}\,f_\mathbf{k}{}^\alpha(\mathbf{K},\,\Omega)B_{\alpha\gamma}(\hat{\mathbf{k}},\,\hat{\mathbf{k}}_1,\,t)$$

$$\times\, \Phi_{\mathbf{k}_1,\mathbf{k}'}{}^{\gamma\beta}(\mathbf{K},\,\Omega,\,t), \qquad (2.5.3)$$

where

$$\Phi^{\alpha\beta}(\mathbf{R},\,\mathbf{r},\mathbf{r}',\,T,\,t)$$

$$= \int \frac{\mathrm{d}^3K}{(2\pi)^3}\frac{\mathrm{d}^3k}{(2\pi)^3}\frac{\mathrm{d}^3k'}{(2\pi)^3}\frac{\mathrm{d}\Omega}{2\pi}$$

$$\times\, \exp(i\mathbf{K}\cdot\mathbf{R})\exp(i\mathbf{k}\cdot\mathbf{r})\exp(-i\mathbf{k}'\cdot\mathbf{r}')$$

$$\times\, \exp(-i\Omega T)\Phi_{\mathbf{k},\mathbf{k}'}{}^{\alpha\beta}(\mathbf{K},\,\Omega,\,t), \quad (2.5.4)$$

$$f_\mathbf{k}{}^\alpha(\mathbf{K},\,\Omega) = G_\alpha\!\left(\mathbf{k}+\frac{\mathbf{K}}{2},\,\omega+\frac{\Omega}{2}\right)G_\alpha{}^*\!\left(\mathbf{k}-\frac{\mathbf{K}}{2},\right.$$

$$\left.\omega - \frac{\Omega}{2}\right). \qquad (2.5.5)$$

Note that Ω is the frequency conjugate to T and not a solid angle.

We are interested primarily in the diffusive part of $\Phi^{\alpha\beta}$. There are functions $\phi_\alpha(\hat{\mathbf{k}})$ and $\psi_\alpha(\hat{\mathbf{k}})$, which we determine in Appendix B, that project out this diffusive part so that the function

$$\Phi(\mathbf{R},\,T,\,t)$$

$$= \int \frac{\mathrm{d}^3k}{(2\pi)^3}\int \frac{\mathrm{d}^3k'}{(2\pi)^3}\,\phi_\alpha(\hat{\mathbf{k}})\Phi_{\mathbf{k},\mathbf{k}'}{}^{\alpha\beta}(\mathbf{R},\,T,\,t)\psi_\beta{}^*(\hat{\mathbf{k}}')$$

$$(2.5.6)$$

satisfies a diffusion equation at $t = 0$. Contributions to Φ can be expanded diagrammatically, as shown in Fig. 12. Each diagram contains double Green-functions lines [representing $f_\mathbf{k}{}^\alpha(\mathbf{R},\,T)$] that are connected by interaction vertices representing scattering events. Diagrams can be classified according to the number N of double Green-function lines. We show below that each double Green-function line can be identified with a step
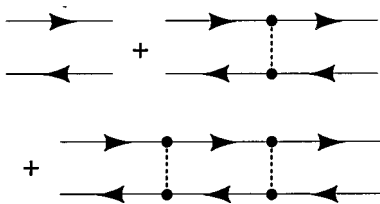

Fig. 12. Diagrammatic representation of $\Phi_{\alpha\beta}$ in terms of ladder diagrams.

of the diffusing photon. Thus Φ can be written as a sum over N of contributions Φ^N arising from all possible walks of N steps:

$$\Phi = \sum_{N=1}^{\infty} \Phi^N. \qquad (2.5.7)$$

Each term Φ^N can be expressed as an integral over all positions of scatterers. Introducing an obvious notation in which 1 refers to all arguments with subscript 1, we can write its Fourier transform as

$$\Phi^N(\mathbf{K},\,\Omega,\,t) = \int \mathrm{d}N...\mathrm{d}1\,\phi(N)f(n)s(n)$$

$$\times \prod_{i=1}^{N-1} B(i+1,\,i)f(i)s(i)\psi(1),$$

$$(2.5.8)$$

where $\mathrm{d}1 = \mathrm{d}T_1\mathrm{d}^3R_1\mathrm{d}^3k_1/(2\pi)^3$,

$$s(1) = \exp(-i\mathbf{K}\cdot\mathbf{R}_1)\exp(i\Omega T_1), \qquad (2.5.9)$$

and $f(1)$ is the spatial and the temporal Fourier transform of Eq. (2.5.5):

$$f(1) = f_{\mathbf{k}_1}{}^{\alpha_1}(\mathbf{R}_1,\,T_1), \qquad (2.5.10)$$

$$= \frac{\bar{\epsilon}_{\alpha_1}{}^3}{(4\pi n_{\alpha_1}\cos\,\delta_{\alpha_1}R)^2}\exp(-\cos\,\delta_{\alpha_1}R_1/l_{\alpha_1})(2\pi)^3$$

$$\times\, \delta(\mathbf{k}_1-\mathbf{k_R}^{\alpha_1})\delta(T_1-[R_1/v_{g,\alpha_1}(\hat{\mathbf{R}}_1)]),$$

$$(2.5.11)$$

with

$$\bar{\epsilon}_\alpha{}^3 = \begin{cases} \epsilon_\perp{}^2\epsilon_\parallel & \text{if } \alpha = 1 \\ \epsilon_\perp{}^3 & \text{if } \alpha = 2 \end{cases}. \qquad (2.5.12)$$

Using the above information, we show in Appendix B that $\Phi^N(\mathbf{K}=0,\,\Omega=0,\,t=0) = \Phi^N(0,\,0,\,0)$, for an appropriate choice of ϕ and ψ, can be represented as the integral over all possible paths of a path probability distribution $P^N[\text{path}]$:

$$\phi^N(0,\,0,\,0) = \int \mathrm{d}[\text{path}]P^N[\text{path}]. \qquad (2.5.13)$$

We can then express $\Phi^N(\mathbf{K},\,\Omega,\,t)$ as an average over this distribution:

$$\Phi^N(\mathbf{K},\,\Omega,\,t) = \left\langle \exp\!\left(-i\mathbf{K}\cdot\sum_p \mathbf{R}_p\right)\exp\!\left(+i\Omega\sum_p T_p\right)\right.$$

$$\left.\times \prod_{p=2}^{N} \frac{B_{\alpha_p,\alpha_{p-1}}(\mathbf{k}_p,\,\mathbf{k}_{p-1},\,t)}{B_{\alpha_p,\alpha_{p-1}}(\mathbf{k}_p,\,\mathbf{k}_{p-1},0)}\right\rangle_N,$$

$$(2.5.14)$$

where $\langle\;\rangle_N$ signifies an average over all paths with N scattering events and $T_p = R_p/v_{g\alpha_p}$ is the photon travel time for step p. This expression is similar, but not identical, to expressions[8,45] in the literature for $\Phi(\mathbf{R},\,T,\,t)$. Keeping as usual only the dominant terms in a cumulant expansion, we obtain

$$\Phi^N(\mathbf{K},\,\Omega,\,t) = \exp\{-N[\tfrac{1}{2}K_iK_j\langle R_iR_j\rangle - i\Omega\langle T\rangle$$
$$+ \langle\delta B(t)/B\rangle]\}, \qquad (2.5.15)$$

where

$$\langle R_iR_j\rangle = \frac{1}{N}\sum_{p,p'}\langle R_{pi}R_{p'j}\rangle_N$$

$$= \frac{1}{N}\sum_p\langle R_{pi}R_{pj}\rangle + \frac{2}{N}\sum_{p>p'}\langle R_{pi},R_{p'j}\rangle$$

$$= \langle R_\parallel^2\rangle_N n_i^0 n_j^0 + \tfrac{1}{2}\langle R_\perp^2\rangle_N(\delta_{ij} - n_i^0 n_j^0)$$
$$(2.5.16)$$

is the tensor describing the average mean-square displacement between scattering events,

$$\langle T\rangle = \langle R_p/v_{g\alpha_p}(\hat{\mathbf{k}}_p)\rangle_N \qquad (2.5.17)$$

is the p-independent average time between scattering events, and

$$\left\langle\frac{\delta B(t)}{B}\right\rangle = \left\langle\frac{\delta B_{\alpha_1,\alpha_2}(\mathbf{k}_1,\,\mathbf{k}_2,\,t)}{B_{\alpha_1,\alpha_2}(\mathbf{k}_1,\,\mathbf{k}_2,\,0)}\right\rangle, \qquad (2.5.18)$$

with

$$\delta B_{\alpha_1,\alpha_2}(\mathbf{k}_1,\,\mathbf{k}_2,\,t) = B_{\alpha_1,\alpha_2}(\mathbf{k}_1,\,\mathbf{k}_2,\,0)$$
$$- B_{\alpha_1,\alpha_2}(\mathbf{k}_1,\,\mathbf{k}_2,\,t).$$
$$(2.5.19)$$

In Appendix B we derive analytic expressions for $\langle T\rangle$ and $\langle\delta B(t)/B\rangle$. Although analytic expressions for the mean-square displacements cannot be obtained, in Appendix C we derive formal expressions for these quantities that will permit us to obtain good approximations for them. We begin with $\langle T\rangle$:

$$\langle T\rangle = \frac{8\pi}{c}\frac{[n^3]}{[B]_n}, \qquad (2.5.20)$$

where

$$[B]_n = \sum_{\alpha\beta}\int\frac{\mathrm{d}\Omega_{\mathbf{k}}\mathrm{d}\Omega_{\mathbf{p}}}{(4\pi)^2}n_\alpha^3(\hat{\mathbf{k}})B_{\alpha\beta}(\mathbf{k},\,\mathbf{p},\,0)n_\beta^3(\hat{\mathbf{p}})$$
$$(2.5.21)$$

is the angular and polarization average of $B_{\alpha\beta}(\mathbf{k},\,\mathbf{p},\,0)$ and

$$[n^3] = \frac{1}{2}\sum_\alpha\int\frac{\mathrm{d}\Omega_{\mathbf{k}}}{4\pi}n_\alpha^3(\hat{\mathbf{k}}) \qquad (2.5.22)$$

is a similar average of n^3. Similarly,

$$\left\langle\frac{\delta B(t)}{B}\right\rangle = \frac{1}{[B]_n}\sum_{\alpha\beta}\int\frac{\mathrm{d}\Omega_{\mathbf{k}}\mathrm{d}\Omega_{\mathbf{p}}}{(4\pi)^2}n_\alpha^3(\hat{\mathbf{k}})[B_{\alpha\beta}(\mathbf{k},\,\mathbf{p},\,0)$$

$$- B_{\alpha\beta}(\mathbf{k},\,\mathbf{p},\,t)]n_\beta^3(\hat{\mathbf{p}}). \qquad (2.5.23)$$

The sum over N to obtain $\Phi(\mathbf{K},\Omega,t)$ is easily done. The result in the small $\mathbf{k}$, Ω, and t limit is

$$\Phi(\mathbf{K},\,\Omega,\,t) = \frac{1}{\langle T\rangle}\mathcal{D}(\mathbf{K},\,\Omega,\,t), \qquad (2.5.24)$$

where

$$\mathcal{D}(\mathbf{K},\,\Omega,\,t) = \frac{1}{-i\Omega + D_\parallel K_\parallel^2 + D_\perp K_\perp^2 + \mu(t)}$$
$$(2.5.25)$$

is the diffusion propagator, with

$$D_\parallel = \frac{1}{2}\frac{\langle R_\parallel^2\rangle}{\langle T\rangle} = \frac{c}{16\pi}\frac{\langle R_\parallel^2\rangle[B]_n}{[n^3]},$$

$$D_\perp = \frac{1}{4}\frac{\langle R_\perp^2\rangle}{\langle T\rangle} = \frac{c}{32\pi}\frac{\langle R_\perp^2\rangle[B]_n}{[n^3]}, \qquad (2.5.26)$$

$$\mu(t) = \frac{1}{\langle T\rangle}\left\langle\frac{\delta B}{B}\right\rangle = \frac{c}{8\pi}\frac{[\delta B]_n}{[n^3]}. \qquad (2.5.27)$$

Equations (2.5.17)–(2.5.27) completely characterize diffusive transport and DWS in a uniaxial anisotropic medium. Using Eqs. (2.5.2), (2.5.24), and (2.5.25), we obtain the diffusion equation (1.2.2) in real space after Fourier transforming with respect to Ω and $\mathbf{K}$.

In isotropic systems with a single direction-independent index of refraction n, $\langle T\rangle$ and the isotropic diffusion constant are normally expressed as

$$\langle T\rangle = \frac{nl}{c}, \qquad D = \frac{1}{3}\frac{c}{n}l^*, \qquad (2.5.28)$$

where l and l^* are, respectively, the mean free and the transport mean free paths of the diffusing light. To make contact with these isotropic formulas, it is useful to introduce an average index of refraction $\bar{n}$, an average mean free path $\bar{l}$, and transport mean free paths $l_\parallel^*$ and $l_\perp^*$ such that

$$\langle T\rangle = \frac{\bar{n}}{c}\bar{l}, \qquad (2.5.29)$$

$$D_\parallel = \frac{1}{3}\frac{c}{\bar{n}}l_\parallel^*, \qquad D_\perp = \frac{1}{3}\frac{c}{\bar{n}}l_\perp^*. \qquad (2.5.30)$$

Using Eq. (2.4.6), we can define $\bar{l}$ by means of

$$\frac{4\pi}{\bar{l}} = \frac{1}{2[n^2]}\sum_\alpha\int\frac{\mathrm{d}\Omega_k}{4\pi}\frac{4\pi n_\alpha^2(\hat{\mathbf{k}})}{l_\alpha(\hat{\mathbf{k}})} = \frac{1}{2}\frac{[B]_n}{[n^2]}.$$
$$(2.5.31)$$

Then $\langle T\rangle = (\bar{l}/c)([n^3]/[n^2])$, and

$$\bar{n} = \frac{[n^3]}{[n^2]}. \qquad (2.5.32)$$

Similarly, $D_\parallel = (c/2\bar{n})(\langle R_\parallel^2\rangle/\bar{l})$, and $D_\perp = (c/4\bar{n})$ $\times (\langle R_\perp^2\rangle/\bar{l})$. Thus we can define $l_\parallel^*$ and $l_\perp^*$ by using

$$\langle R_\parallel^2\rangle = \frac{2}{3}\bar{l}l_\parallel^*, \qquad \langle R_\perp^2\rangle = \frac{4}{3}\bar{l}l_\perp^*. \qquad (2.5.33)$$

In an isotropic system, $\bar{l}$ reduces to l, $\bar{n}$ to n, and $l_\parallel^* = l_\perp^*$ to l^*. In nematics $\bar{l}$ tends to zero as $H \to 0$, whereas $l_\parallel^*$ and $l_\perp^*$ do not. Thus both the average time $\langle T\rangle$ and the mean-square displacements $\langle R_\parallel^2\rangle$ and $\langle R_\perp^2\rangle$ tend to zero in this limit, but the ratios $\langle R_\parallel^2\rangle/\langle T\rangle$ and $\langle R_\perp^2\rangle/\langle T\rangle$ do not.

The dynamic absorption coefficient $\mu(t)$ can be expressed in terms of these new variables as

$$\mu(t) = \frac{c}{n\bar{l}} \frac{[\delta B(t)]_n}{[B]_n}. \qquad (2.5.34)$$

In isotropic systems, $[\delta B(t)]_n/[B]_n = 2k_0^2 D_s t(l/l^*)$, and $\mu(t) = (2c/nl^*)Dk_0^2 t$. In liquid crystals, Eq. (2.5.34) is not so useful because the mode frequencies Γ_q are proportional to B, as indicated in Eq. (2.3.4). As a result,

$$[\delta B(t)]_n/t = (\Delta\epsilon)^2 k_B T \frac{\omega^4}{c^4} \sum_{\alpha,\beta,\delta}$$

$$\times \int \frac{d\Omega_k}{4\pi} \frac{d\Omega_p}{4\pi} \frac{n_\alpha^3(\hat{\mathbf{k}})N(\mathbf{e}_\alpha, \mathbf{e}_\beta, \hat{\mathbf{u}}_\delta)n_\beta^3(\hat{\mathbf{p}})}{\eta_\delta(\mathbf{q})}$$

$$= (\Delta\epsilon)^2 \frac{\omega^4}{c^4} k_B T \sum_\delta \left[\frac{N}{\eta_\delta}\right]_n, \qquad (2.5.35)$$

where $\mathbf{q} = n_\alpha\mathbf{k} - n_\beta\mathbf{p}$, depends only on viscosities and not on Frank elastic constant K_i or the magnetic field. The average $[N/\eta_\delta]_n$ is defined by Eq. (2.5.21), with B being replaced by N/η_δ.

The evaluation of $\langle R_\parallel^2 \rangle$ and $\langle R_\perp^2 \rangle = 2\langle R_x^2 \rangle$ is outlined in Appendix C. The exact expressions for these quantities involve the inversion of infinite-dimensional matrices. If we approximate these matrices by their lowest nonvanishing terms, we obtain the following expression for the photon diffusion coefficient:

$$D_\parallel = \frac{4\pi c}{n_2^5(2+\eta)} \left(\frac{4\pi}{3}\right)^2 \frac{\mathcal{B}_{11}^z + \mathcal{B}_{22}^z - 2\mathcal{B}_{12}^z}{\det \mathcal{B}^z}$$

$$D_\perp = \frac{4\pi c}{n_2^5(2+\eta)} \left(\frac{4\pi}{3}\right)^2$$

$$\times \frac{(1+\eta)\mathcal{B}_{11}^x + \mathcal{B}_{22}^x - 2\sqrt{1+\eta}\mathcal{B}_{12}^x}{(1+\eta)\det \mathcal{B}^x},$$

$$(2.5.36)$$

where $\eta = \Delta\epsilon/\epsilon_\perp$,

$$\mathcal{B}_{\alpha\beta}^z = \int dC dC' d\phi d\phi' [C^2 - CC']B_{\alpha\beta}(C, C', \phi, \phi'),$$

$$(2.5.37)$$

$$\mathcal{B}_{\alpha\beta}^x = \int dC dC' d\phi d\phi' [(1-C^2)\cos^2\phi$$

$$- \sqrt{1-C^2}\sqrt{1-C'^2}$$

$$\times \cos\phi\cos\phi']B_{\alpha\beta}(C, C', \phi, \phi'), \qquad (2.5.38)$$

with

$$C \equiv C_\mathbf{k} = n_1(\hat{\mathbf{k}})\cos\theta_\mathbf{k}/n_2. \qquad (2.5.39)$$

The full expression for $B_{\alpha\beta}(C, C', \phi, \phi')$ is given in Appendix C.

To discuss the diffusion constants $D_\parallel$ and $D_\perp$, we introduce a factor

$$D_0 = 3\pi \frac{c^3}{\omega^2 n_2^3} \frac{K_3}{k_B T} \frac{\epsilon_\perp^2}{(\Delta\epsilon)^2}, \qquad (2.5.40)$$

which gives the order of magnitude of the diffusion constants, and write

$$D_\parallel = D_0\tilde{D}_\parallel, \qquad D_\perp = D_0\tilde{D}_\perp. \qquad (2.5.41)$$

The numerical factors $\tilde{D}_\parallel$ and $\tilde{D}_\perp$ depend only on the ratios of the Frank elastic constants (K_1/K_3 and K_2/K_3) and on the relative dielectric anisotropy $\Delta\epsilon/\epsilon_\perp$. With the material parameters of the nematic compound CB15 ($\Delta\epsilon/\epsilon_\perp = 0.228$, $n_2 = 1.543$, $K_3 = 5.3 \times 10^{-7}$ dyn), green light ($\omega/c = 1.15 \times 10^5$ cm^{-1}), and a temperature $T = 300$ K we obtain $D_0 = 1.5 \times 10^9$ cm^2/s.

For 5CB we show in Fig. 13 how the diffusion constants $\tilde{D}_\parallel$ and $\tilde{D}_\perp$ and the relative anisotropy $(D_\parallel - D_\perp)/D_\perp$ behave in a magnetic field. $\tilde{D}_\parallel$ and $\tilde{D}_\perp$ grow with H because the magnetic field suppresses director fluctuations. The field dependence of the relative anisotropy in the diffusion is weak. For ordinary magnetic fields up to 5×10^4 G, which corresponds to a magnetic coherence length ξ_3 of approximately 1 μm, the changes in $\tilde{D}_\parallel$ and $\tilde{D}_\perp$ are small. The values for $H = 0$ read $\tilde{D}_\parallel = 0.95$ and $\tilde{D}_\perp = 0.65$, with a ratio $\tilde{D}_\parallel/\tilde{D}_\perp = 1.45$. Taking these values together with $D_0 = 1.5 \times 10^9$ cm^2/s, we obtain $D_\parallel = 1.43 \times 10^9$ cm^2/s and $D_\perp = 0.98 \times 10^9$ cm^2/s. These values are in excellent agreement with the numerical simulations on which we report in Subsection 2.F. The ratio $\tilde{D}_\parallel/\tilde{D}_\perp$ is also in good agreement with experiments. However, the absolute values of $D_\parallel$ and $D_\perp$ are larger by a factor of 2. We attribute this partially to the fact that the experiments used light with a longer wavelength. Note, again, that both diffusion constants are finite for $H \to 0$, although the scattering mean free path for extraordinary-to-extraordinary scattering goes to zero.

In Fig. 14 we explore the anisotropy in the diffusion as a function of the dielectric anisotropy $\Delta\epsilon/\epsilon_\perp$. We set $K_1 = K_2 = K_3$. Even at $\Delta\epsilon = 0$, the diffusion constants $D_\parallel$ and $D_\perp$ are slightly different because of the inherent anisotropy in the nematic structure factor. The anisotropy in the diffusion grows with $\Delta\epsilon$ because the speed of light of the extraordinary light ray is larger along the di-
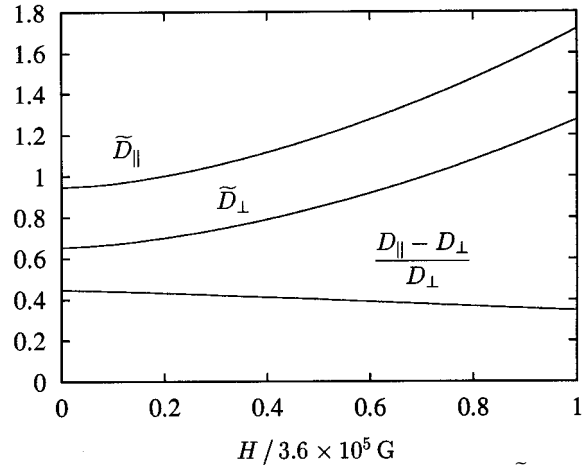

Fig. 13. Field dependence of the diffusion constants $\tilde{D}_\parallel$ and $\tilde{D}_\perp$ and the relative anisotropy $(D_\parallel - D_\perp)/D_\perp$ for the nematic compound 5CB ($K_1/K_3 = 0.79$, $K_2/K_3 = 0.43$, and $\Delta\epsilon/\epsilon_\perp = 0.228$).
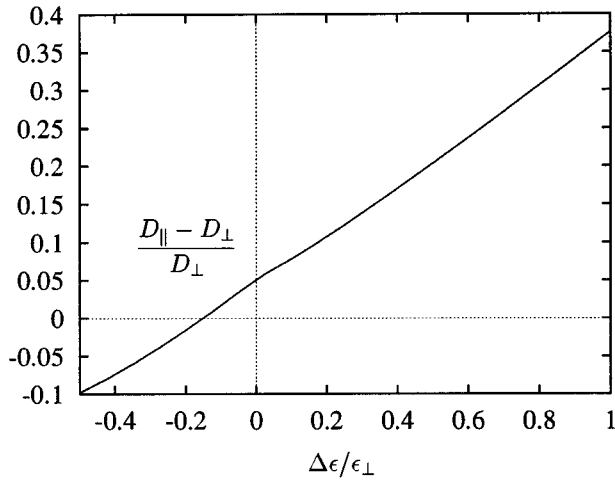
Fig. 14. Relative anistropy $(D_\parallel - D_\perp)/D_\perp$ as a function of $\Delta\epsilon/\epsilon_\perp$ for $K_1 = K_2 = K_3$.
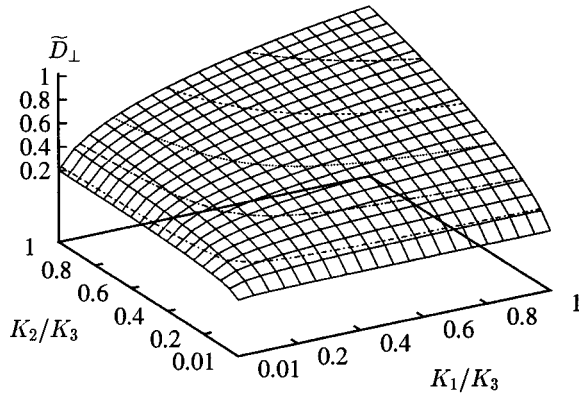

Fig. 15. Reduced diffusion constant $\tilde{D}_\perp$ as a function of K_1/K_3 and K_2/K_3 for $\Delta\epsilon = 0$.

rector than perpendicular to it. In contrast, for $\Delta\epsilon/\epsilon_\perp < -0.15$, the anisotropy $(D_\parallel - D_\perp)/D_\perp$ changes sign, and light diffuses faster perpendicular to the director. This effect and the inversion point $D_\parallel = D_\perp$ should be observable in discotic nematics where $\Delta\epsilon$ is negative.

Finally, we discuss the dependence of the diffusion on the elastic constants K_1/K_3 and K_2/K_3. We show in Fig. 15 that, since the light scattering from the director modes increases, $\tilde{D}_\perp$ decreases with the elastic constants. At the extreme values $K_1/K_3 = K_2/K_3 = 0.01$, we obtain $\tilde{D}_\perp = 0.07$. The contour lines reveal an asymmetry between the splay (K_1) and the twist (K_2) distortions. $\tilde{D}_\perp$ decreases more strongly with K_2/K_3. The diffusion constant $\tilde{D}_\parallel$ shows a similar behavior. Figure 16 gives the anisotropy $(D_\parallel - D_\perp)/D_\perp$ for the same range. It grows with decreasing elastic constants, showing that $\tilde{D}_\perp$ is more affected by splay and twist distortions than is $\tilde{D}_\parallel$. The asymmetry between splay and twist is clearly visible. Figures 15 and 16 cover the range of conventional thermotropic nematics where usually $K_1/K_3 < 1$ and $K_2/K_3 < 1$.

Until now, we have concentrated on the scalar photon diffusion propagator. The polarization and direction de-

pendence of diffusing photons are also of interest. We show in Appendix B that the function

$$\Phi_{\hat{\mathbf{k}},\hat{\mathbf{k}}'}{}^{\alpha\beta}(\mathbf{K},\,\Omega,\,t) = \int \frac{k^2 dk}{(2\pi)^3}\frac{k'^2 dk'}{(2\pi)^3}\,\Phi_{\mathbf{k},\mathbf{k}'}{}^{\alpha\beta}(\mathbf{K},\,\Omega,\,t),$$
$$(2.5.42)$$

which determines the intensity of diffused radiation with polarization α and phase direction $\hat{\mathbf{k}}$ produced by a source of radiation with polarization β and phase direction $\hat{\mathbf{k}}'$, satisfies

$$\phi_{\hat{\mathbf{k}}\hat{\mathbf{k}}'}{}^{\alpha\beta}(\mathbf{k},\,\Omega,\,t) = \frac{1}{(4\pi)^2}\frac{c}{8\pi}\frac{n_\alpha{}^3(\hat{\mathbf{k}})n_\beta{}^3(\hat{\mathbf{k}}')}{[n^3]}\,\mathcal{D}(\mathbf{K},\,\Omega,\,t).$$
$$(2.5.43)$$

From this we can calculate the polarization dependence of the intensity of output radiation. In particular, using Eq. (2.2.22) for the Poynting vector, we obtain

$$R = \frac{|\mathbf{S}_1(\hat{\mathbf{k}})|}{|\mathbf{S}_2(\hat{\mathbf{k}})|} = \frac{1}{\cos\delta_1(\hat{\mathbf{k}})}\frac{n_1{}^2(\hat{\mathbf{k}})}{n_2{}^2}\qquad(2.5.44)$$

for the ratio of output intensity of the extraordinary ray to that of the ordinary ray propagating along the direction $\mathbf{v}_{g1}(\hat{\mathbf{k}})$. This ratio is independent of the polarization state of the input radiation.

F. Numerical Simulations

To complete our experimental and theoretical investigation of light diffusion in the nematic phase, we performed numerical simulations. How does the photon distribution evolve if we launch photons uniformly along the x direction and perpendicular to the director, which we choose parallel to the z axis? Initially, after relatively few scattering events, the photon cloud will be asymmetric, still indicating the initial direction of the photons. As time passes, the photons experience further scattering events and lose their memory of their initial direction. As a result, the cloud becomes more symmetric, although it will be elongated or flattened along the z axis as a re-
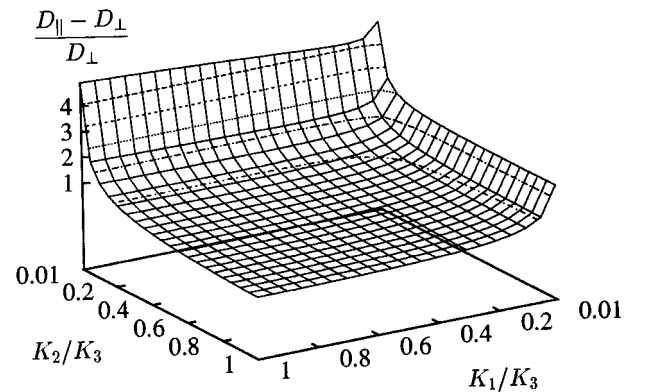

Fig. 16. Relative anisotropy $(D_\parallel - D_\perp)/D_\perp$ as a function of K_1/K_3 and K_2/K_3 for $\Delta\epsilon = 0$.
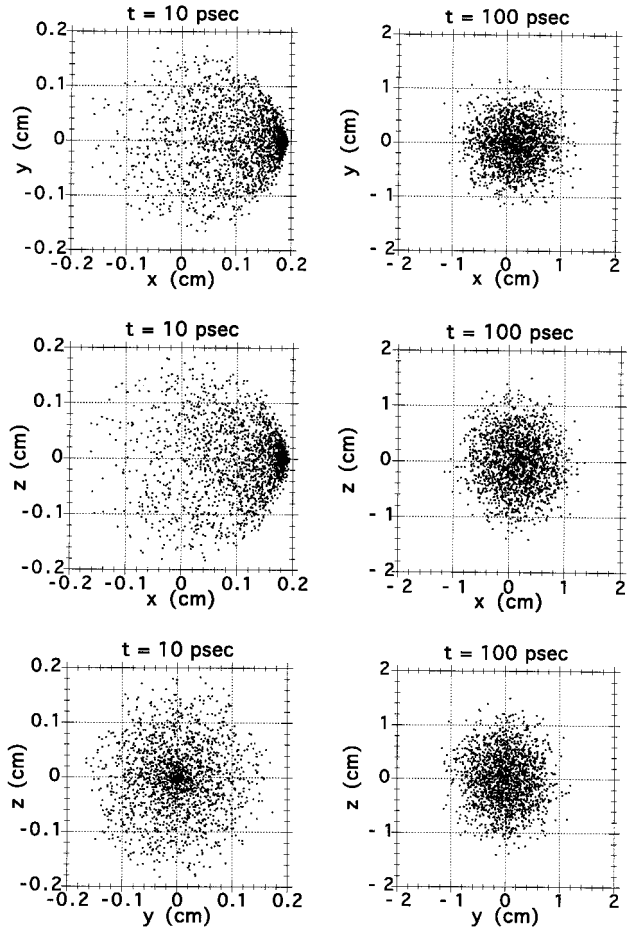
Fig. 17. Clouds of photons projected on the xy, the xz, and the yz planes for times $t = 10$ ps (left-hand column) and $t = 100$ ps.

sult of the anisotropic diffusion. At this stage the distribution $\rho(x, y, z)$ of the photon positions is Gaussian, i.e.,

$$\rho(x, y, z) = \frac{1}{(2\pi)^{3/2}} \frac{1}{\sigma_x \sigma_y \sigma_z} \exp\left[-\frac{(x - x_0)^2}{2\sigma_x^2} \right.$$

$$\left. -\frac{(y - y_0)^2}{2\sigma_y^2} - \frac{(z - z_0)^2}{2\sigma_z^2} \right], \quad (2.6.1)$$

where the diffusion constants follow from

$$\sigma_x^2 = 2D_x t, \qquad \sigma_y^2 = 2D_y t, \qquad \sigma_z^2 = 2D_z t. \quad (2.6.2)$$

The positions x_0, y_0, and z_0 define the true starting point for a diffuse photon source.

In our simulations we placed 2000 photons at the origin, half of them with ordinary and the other half with extraordinary polarization. Then we let them propagate along the positive x axis for a time $dt = 0.1$ ps, which was chosen such that the traveled distance $ds = v_{g\alpha} dt \approx 2 \times 10^{-3}$ cm was much smaller than the scattering mean free path. We note that photons transport energy and that therefore they travel along the Poynting vector $\mathbf{S}_\alpha$ with the group velocity $v_{g\alpha}$. The direction of $\mathbf{S}_\alpha$ is different from the wave vector $\mathbf{k}^\alpha$, as explained in Subsection

2.B. After each time step we checked for scattering events. A photon was scattered if a random number generated between 0 and 1 was smaller than the scattering probability $ds \cos \delta_\alpha / l_\alpha(\hat{\mathbf{k}})$ [see Appendix B and Eq. (B4)]. We then determined the new polarization mode and wave vector of the scattered photon by using the conditional probability $\pi(\mathbf{k}_2, \alpha_2|\mathbf{k}_1, \alpha_1)$ for a scattering event from polarization α_1 and phase direction $\hat{\mathbf{k}}_1$ to polarization α_2 and phase direction $\hat{\mathbf{k}}_2$ [see Appendix B and Eq. (B6)]. The conditional probability depends on the differential cross section, which is proportional to the structure factor $B_{\alpha_2, \alpha_1}(\hat{\mathbf{k}}_2, \hat{\mathbf{k}}_1, 0)$. We used reported data on 5CB for the calculations.

In Fig. 17 we show projections of the photon cloud on the xy, xz, and yz planes for times $t = 10$ ps (left-hand column) and $t = 100$ ps (right-hand column). At $t = 10$ ps the xy and the xz projections clearly indicate the initial direction of the photons. At $t = 100$ ps the cloud looks symmetric, and in the xz and the yz projections we can sense a slight elongation along the z axis. We fitted several snapshots with the Gaussian distribution $\rho(x, y, z)$ of Eq. (2.6.1). In Fig. 18 we plot the variances σ_x^2, σ_y^2, and σ_z^2 which grow, as expected, linearly in time. The diffusion constants D_x and D_y perpendicular to the director are equal and are smaller than D_z by a fac-
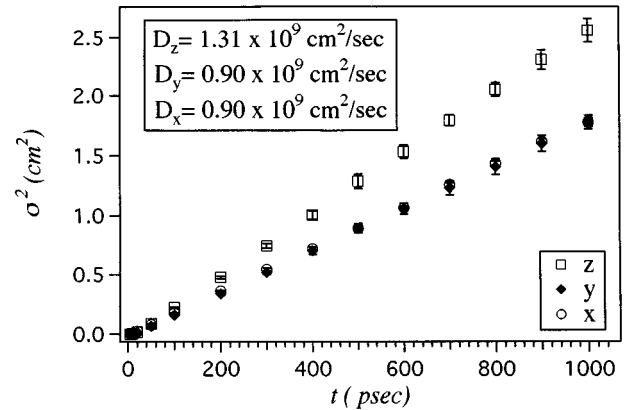

Fig. 18. Variances σ_x^2, σ_y^2, and σ_z^2 for the Gaussian distribution of the photon positions. The upper left-hand inset gives the diffusion constants that follow from the variances.
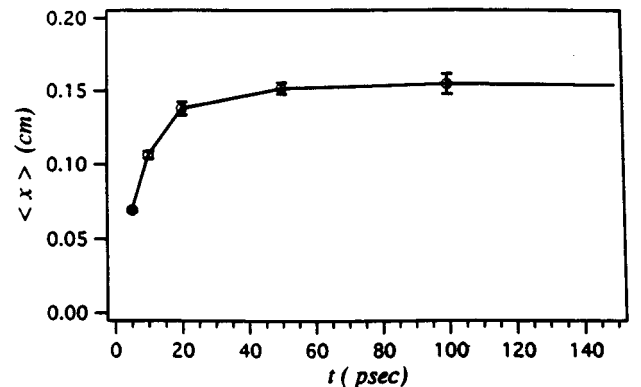

Fig. 19. Averaged photon position $x_0 = \langle x \rangle$ as a function of time. It reaches a constant value of 1.5 mm.

tor of 1.46, which is in excellent agreement with our theoretical prediction and in good agreement with experiment. Interestingly, the center of the photon cloud is not the origin but is shifted in the positive x direction. The distance from the center reaches a constant value of approximately 1.5 mm, as shown in Fig. 19. This is the distance that the photons need to randomize their initial directions and is of the order of the mean free path $l_\perp^*$.

ACKNOWLEDGMENTS

Note added in proof: While this paper was being refereed, a theoretical paper on light diffusion in nematic liquid crystals was published.[47] Its results and conclusions are similar to ours.

APPENDIX A: WEAK-SCATTERING PHOTON GREEN FUNCTION

In this appendix we review briefly the derivation of the weak-scattering form for the single-photon Green function, and we show that the mean free path for extraordinary-to-extraordinary scattering vanishes in the limit $\mathbf{H} \to 0$.[41,46] The average photon Green function can be expanded in powers of fluctuations in the dielectric tensor. In the weak-scattering limit, to which we restrict ourselves in this paper, the only diagrams contributing to G are the noncrossing diagrams shown in Fig. 11. In the weak-scattering limit the photon Green function remains diagonal in the polarization indices α and β (see Refs. 28 and 29), and the inverse Green function becomes

$$G_\alpha^{-1}(\mathbf{k}, \omega) = G_\alpha^{0-1}(\mathbf{k}, \omega) - \Sigma_\alpha(\mathbf{k}, \omega), \qquad \text{(A1)}$$

where

$$\Sigma_\alpha(\mathbf{k}, \omega) = \int \frac{\mathrm{d}^3 q}{(2\pi)^3} B_{\alpha\beta}(\mathbf{k}, \mathbf{q}, 0) G_\beta(\mathbf{q}, \omega) \qquad \text{(A2)}$$

is the photon self-energy and

$$G_\alpha^0(\mathbf{k}, \omega) = \left[\left(\frac{\omega}{c} \right)^2 - \frac{k^2}{n_\alpha^2(\hat{\mathbf{k}})} \right]^{-1} \qquad \text{(A3)}$$

is the bare Green function. Using $\mathrm{Im}\, G_\alpha^0(\mathbf{k}, \omega) = -i(\pi/2)[n_\alpha(\hat{\mathbf{k}})c/\omega]\delta[k - n_\alpha(\hat{\mathbf{k}})(\omega/c)]$ and restricting ourselves to the energy shell with $k = (\omega/c)n_\alpha(\hat{\mathbf{k}})$, we obtain

$$\mathrm{Im}\, G_\alpha^{-1}(\mathbf{k}, \omega) = \frac{\omega}{c} \frac{1}{n_\alpha(\hat{\mathbf{k}})l_\alpha(\hat{\mathbf{k}})}$$

$$= \sum_\beta \int \frac{\mathrm{d}^3 q}{(2\pi)^3} B_{\alpha\beta}(\mathbf{k}_\alpha, \mathbf{q}_\beta) \mathrm{Im}\, G_\alpha^0$$

$$\times (\mathbf{q}, \omega)$$

$$= \sum_\beta \int \frac{\mathrm{d}\Omega_\mathbf{q}}{(2\pi)^3} \frac{\pi}{2} B_{\alpha\beta}(\mathbf{k}_\alpha, \mathbf{q}_\beta) n_\beta^3(\hat{\mathbf{q}}).$$

$$\text{(A4)}$$

This equation is equivalent to Eq. (2.4.6).

The preceding expression shows (1) that the mean free path for ordinary rays is determined entirely by scattering into extraordinary rays because the factor N [Eq. (2.3.12)] in B_{22} is zero, and (2) that the mean free path for extraordinary rays tends to zero as the reciprocal of the logarithm of $\Delta\chi H^2$ because of divergent extraordinary-to-extraordinary scattering. The latter follows because $\mathbf{q}_s$ is zero when $\alpha = \beta$ and when $\hat{\mathbf{k}}_\alpha = \hat{\mathbf{q}}_\alpha$. $B_{11}(\hat{\mathbf{k}}, \hat{\mathbf{q}}, 0)$ in the neighborhood of $\hat{\mathbf{q}} = \hat{\mathbf{k}}$ can be expressed as

$$B_{11} \approx T \frac{4(\Delta\epsilon)^2}{\epsilon_\parallel^2 \epsilon_\perp^2} \frac{\omega^2}{c^2} \frac{1}{K_1 n_1^2(\hat{\mathbf{k}})}$$

$$\times \frac{1}{\sin^2 \theta_\mathbf{k}(\delta\theta_\mathbf{q})^2 + C(\hat{\mathbf{k}})(\delta\phi_\mathbf{q})^2 + [\Delta\chi H^2/K_1(\omega/c)^2 n_1^2(\hat{\mathbf{k}})]},$$
$$\text{(A5)}$$

where $C(\hat{\mathbf{k}})$ is a well-behaved function of $\theta_\mathbf{k}$ and $\phi_\mathbf{k}$ and where we used $N(\mathbf{e}_1, \mathbf{e}_1, \mathbf{u}_1) = 4\cos^2(\theta_\mathbf{k} - \theta_\mathbf{q}) \approx 4$. Using this in Eq. (A4), we obtain

$$\frac{4\pi}{l_1(\hat{\mathbf{k}})} \approx T \frac{(\Delta\epsilon)^2}{\pi\epsilon_\parallel^2 \epsilon_\perp^2} \frac{\omega^2}{c^2} \frac{n_1^2(\hat{\mathbf{k}})}{\sqrt{C(\hat{\mathbf{k}})}} \ln\left[\frac{\Delta\chi H^2}{K_1(\omega/c)^2 n_1^2(\hat{\mathbf{k}})} \right].$$
$$\text{(A6)}$$

Thus the mean free path for extraordinary-to-extraordinary scattering tends to zero as H tends to zero. The transport mean free path is, however, finite in this limit.

APPENDIX B: PATH INTEGRALS FOR PHOTON DIFFUSION

In this appendix we fill in the missing steps between Eqs. (2.5.12) and (2.5.13). The integral over $\mathrm{d}T_i$ in Eq. (2.5.11) is trivial; it sets $T_i = R_i/v_{g,\alpha_i}$ in $s(i)$, i.e., it sets the travel time to the distance divided by the group velocity. The propagator $f(1)$ has a delta function setting $\mathbf{k}$ equal to $\mathbf{k_R}^\alpha$, the wave vector corresponding to energy propagation along $\mathbf{R}$. In addition, f has a factor of R^{-2}. These two factors simplify integrals over $\mathbf{R}$ and $\mathbf{k}$:

$$\int \frac{\mathrm{d}^3 R \, \mathrm{d}^3 k}{(2\pi)^3} \frac{(2\pi)^3}{R^2} \delta(\mathbf{k} - \mathbf{k_R}^\alpha)$$

$$\to \int \mathrm{d}R \, \mathrm{d}\Omega_k \frac{\mathrm{d}\Omega_R^\alpha}{\mathrm{d}\Omega_k^\alpha} \delta[k - c/n_\alpha(\hat{\mathbf{k}})], \qquad \text{(B1)}$$

where Ω_R^α and Ω_k^α are, respectively, the solid angles associated with $\mathbf{R}$ and $\mathbf{k}$ for the wave with polarization α with Jacobian

$$\frac{\mathrm{d}\Omega_R^\alpha}{\mathrm{d}\Omega_k^\alpha} = \frac{\mathrm{d}\cos\theta_R}{\mathrm{d}\cos\theta_k} = \frac{n_\alpha^6}{\epsilon_\alpha^3} \cos^3\delta_\alpha, \qquad \text{(B2)}$$

where we used Eq. (2.5.12) and, for $\alpha = 1$, we used Eq. (2.3.14). The B and the f factors can now be combined to yield

$$B(2, 1)f(1) \rightarrow \frac{1}{(4\pi)^2} B_{\alpha_2\alpha_1}(\hat{\mathbf{k}}_2, \hat{\mathbf{k}}_1, t)n_{\alpha_1}{}^4(\hat{\mathbf{k}}_1)$$

$$\times \cos \delta_{\alpha_1} \exp[-R_1 \cos \delta_{\alpha_1}/l_{\alpha_1}(\hat{\mathbf{k}}_1)]$$

$$= \frac{B_{\alpha_2\alpha_1}(\hat{\mathbf{k}}_2, \hat{\mathbf{k}}_1, t)n_{\alpha_1}{}^3(\hat{\mathbf{k}}_1)}{Z_{\alpha_1}(\hat{\mathbf{k}}_1)} p_{\alpha_1}(R_1), \qquad \text{(B3)}$$

where

$$p_\alpha(R)\mathrm{d}R = \frac{\exp[-R \cos \delta_\alpha/l_\alpha(\hat{\mathbf{k}})]}{l_\alpha(\hat{\mathbf{k}})/\cos \delta_\alpha} \mathrm{d}R \qquad \text{(B4)}$$

is the probability that light with polarization α starting at $R = 0$ and traveling in the direction $\mathbf{k}_R{}^\alpha$ undergoes a scattering event in the interval $(R, R + \mathrm{d}R)$, and where

$$Z_\alpha(\hat{\mathbf{k}}) = (4\pi)^2[n_\alpha(\hat{\mathbf{k}})l_\alpha(\hat{\mathbf{k}})]^{-1}$$

$$= \sum_\beta \int \mathrm{d}\Omega_{\mathbf{k}'} B_{\alpha\beta}(\hat{\mathbf{k}}, \hat{\mathbf{k}}', t = 0)n_\beta{}^3(\hat{\mathbf{k}}'). \qquad \text{(B5)}$$

Thus we can define the conditional probability

$$\pi(\mathbf{k}_2, \alpha_2|\mathbf{k}_1, \alpha_1) = \frac{n_{\alpha_2}{}^3(\mathbf{k}_2)B_{\alpha_2,\alpha_1}(\hat{\mathbf{k}}_2, \hat{\mathbf{k}}_1, 0)}{Z_{\alpha_1}(\hat{\mathbf{k}}_1)} \qquad \text{(B6)}$$

that light scatters from polarization α_1 and phase direction $\hat{\mathbf{k}}_1$ to polarization α_2 and phase direction $\hat{\mathbf{k}}_2$. This probability satisfies the required normalization condition

$$\sum_{\alpha_2} \int \mathrm{d}\Omega_{\mathbf{k}_2}\pi(\hat{\mathbf{k}}_2, \alpha_2|\hat{\mathbf{k}}_1, \alpha_1) = 1. \qquad \text{(B7)}$$

We can now show, with an appropriate choice of $\phi(1)$ and $\psi(1)$, that the integrand I^N of $\Phi^N(0, 0, 0)$ in Eq. (2.5.8) is an N-independent constant times the normalized probability distribution for paths with N scattering events. To be explicit, consider $\Phi^4 = \int \mathrm{d}1 \ldots \mathrm{d}4 I^4$, where, again with an obvious shorthand-notation,

$$I^4 = \phi(4)\frac{p(4)n^3(4)}{Z(4)} \frac{B(4, 3)n^3(3)p(3)}{Z(3)}$$

$$\times \frac{B(3, 2)n^3(2)p(2)}{Z(2)} \frac{B(2, 1)n^3(1)p(1)}{Z(1)} \psi(1), \qquad \text{(B8)}$$

where now $1 = (\mathbf{R}_1, \Omega_{k_1}, \alpha_1)$ refers to those variables that remain after integration over k_1 and $\Omega_{\mathbf{R}_1}$. With the choice $\phi(1) = \psi(1) = AZ(1)$, this function can be written as

$$I^4 = A^2 p(4)\pi(4|3)p(3)n^3(3)B(3, 2)n^3(2)p(2)$$

$$\times \pi^T(2|1)p(1), \qquad \text{(B9)}$$

where $\pi^T(2|1) = \pi(1|2)$ is the operator transpose of $\pi(1|2)$. The variables $1, \ldots, 4$ define the distance traveled and the direction and the polarization of light of each of the four steps that we are considering; i.e., they define a particular light path, and I^4 can be regarded as a function of path. Then

$$\Phi^4(0, 0, 0) = \int \mathrm{d}[\text{path}]I^4[\text{path}]$$

$$= A^2 \int \mathrm{d}2\mathrm{d}3n^3(3)B(3, 2)n^3(2)$$

$$= A^2 \sum_{\alpha_3\alpha_2} \int \mathrm{d}\Omega_{\mathbf{k}_3}\mathrm{d}\Omega_{\mathbf{k}_4}n_{\alpha_3}{}^3(\hat{\mathbf{k}}_3)B_{\alpha_3,\alpha_2}$$

$$\times (\mathbf{k}_3, \mathbf{k}_2, 0)n_{\alpha_2}{}^3(\hat{\mathbf{k}}_2) \equiv A^2(4\pi)^2[B]_n, \qquad \text{(B10)}$$

where $\mathrm{d}[\text{path}] = \mathrm{d}1\mathrm{d}2\mathrm{d}3\mathrm{d}4$, $[B]_n$ is defined in Eq. (2.5.21), and where we used the normalization condition Eq. (B7) to carry out the integrals over 1 and 4. Note that $[B]_n$ scales as an index of refraction squared. Thus, choosing $4\pi A = [B]_n^{-1/2}$, we can define the probability for a given path with four scattering events to be

$$P^4[\text{path}] = I^4[\text{path}]. \qquad \text{(B11)}$$

This probability consists of products of conditional probabilities $\pi(a|b)$ for scattering from b to a and a single joint probability:

$$\mathcal{P}(a, b) = \frac{p(a)n^3(a)B(a, b)n^3(b)p(b)}{(4\pi)^2[B]_n} \qquad \text{(B12)}$$

for scattering from b to a or from a to b. The joint and the conditional probabilities satisfy the relation $\pi(4|3)\mathcal{P}(2, 1) = \mathcal{P}(4, 3)\pi^T(2|1)$. Thus P^4 can be expressed in any of the following equivalent forms:

$$P^4 = p(4)\pi(4|3)\mathcal{P}(3, 2)\pi^T(2|1)p(1)$$

$$= \mathcal{P}(4, 3)\pi^T(3|2)p(2)\pi^T(2|1)p(1)$$

$$= p(4)\pi(4|3)p(3)\pi(3|2)\mathcal{P}(2, 1). \qquad \text{(B13)}$$

These equations are easily generalized to arbitrary N:

$$P^N = \prod_{s=k+1}^{N} p(s)\pi(s|s-1)\mathcal{P}(k, k-1)$$

$$\times \prod_{s=1}^{k-2} \pi^T(s+1|s)p(s), \qquad \text{(B14)}$$

where k is any integer from 2 to N.

The above form for P^N can now be used to calculate $\langle T \rangle$, $\langle \delta B(t)/B \rangle$, and $\langle R_\parallel{}^2 \rangle$, $\langle R_x{}^2 \rangle$. We begin with $\langle T \rangle$. For arbitrary step a, we have

$$\langle T \rangle = \int \mathrm{d}[\text{path}]P^N[\text{path}]R_a/v_g(a)$$

$$= \frac{1}{(4\pi)^2[B]_n} \int \mathrm{d}1\mathrm{d}2p(1)(R_1/v_{g1})\mathcal{P}(1, 2)p(2)$$

$$= \frac{1}{[B]_n} \sum_{\alpha_1,\alpha_2} \int \frac{\mathrm{d}\Omega_{\mathbf{k}_1}\mathrm{d}\Omega_{\mathbf{k}_2}}{(4\pi)^2} \frac{l_{\alpha_1}(\hat{\mathbf{k}}_1)}{\cos \delta_{\alpha_1}(\hat{\mathbf{k}}_1)v_{g,\alpha_1}(\hat{\mathbf{k}}_1)}$$

$$\times n_{\alpha_1}{}^3(\hat{\mathbf{k}}_1)B_{\alpha_1\alpha_2}(\mathbf{k}_1, \mathbf{k}_2, 0)n_{\alpha_2}{}^3(\mathbf{k}_2)$$

$$= \frac{8\pi}{c} \frac{[n^3]}{[B]_n}, \qquad \text{(B15)}$$

where $[n^3]$ is defined as in Eq. (2.5.22) and where we used Eq. (2.4.6) for $l_\alpha(\hat{\mathbf{k}})$ and Eq. (2.2.21), relating $v_{g\alpha_1}\cos\delta_{\alpha_1}$ to $c/n_{\alpha_1}(\hat{\mathbf{k}})$. Similarly,

$$\langle\delta B(t)/B\rangle = \int \mathrm{d}[\mathrm{path}]P^N[\mathrm{path}]\delta B/B$$

$$= \frac{1}{[B]_n}\sum_{\alpha\beta}\int\frac{\mathrm{d}\Omega_{\mathbf{k}}\mathrm{d}\Omega_{\mathbf{p}}}{(4\pi)^2}n_\alpha{}^3(\hat{\mathbf{k}})[B_{\alpha\beta}(\mathbf{k},\,\mathbf{p},\,0)$$

$$- B_{\alpha\beta}(\mathbf{k},\,\mathbf{p},\,t)]n_\beta{}^3(\hat{\mathbf{p}}) = \frac{[\delta B(t)]_n}{[B]_n}.$$

$$\text{(B16)}$$

We now turn to the calculation of $\Phi_{\hat{\mathbf{k}}\hat{\mathbf{k}}'}{}^{\alpha\beta}(\mathbf{K},\,\Omega,\,t)$ introduced in Eq. (2.5.43). First consider the function

$$\Phi_{\hat{\mathbf{k}}\hat{\mathbf{k}}'}{}^{N,\alpha\beta}(\mathbf{K},\,0,\,0) = \int \mathrm{d}N\,\ldots\,\mathrm{d}1 h_{\alpha\alpha_N}(\Omega_{\mathbf{k}},\,\Omega_{\mathbf{k}_N})$$

$$\times f(N)s(N)\prod_{i=1}^{N-1}B(i+1,\,i)f(1)s(1)$$

$$\times h_{\alpha_1\beta}(\Omega_{\mathbf{k}_1},\,\Omega_{\mathbf{k}'})$$

$$= \frac{(4\pi)^2[B]_n}{Z_\alpha(\hat{\mathbf{k}})Z_\beta(\hat{\mathbf{k}}')}\Bigg\langle h_{\alpha\alpha_N}(\Omega_{\mathbf{k}},\,\Omega_{\mathbf{k}'})$$

$$\times \exp\!\left(-i\mathbf{K}\cdot\sum_p\mathbf{R}_p\right)h_{\alpha_1\beta}$$

$$\times (\Omega_{\mathbf{k}_1},\,\Omega_{\mathbf{k}'})\Bigg\rangle_N$$

$$\approx \frac{(4\pi)^2[B]_n}{Z_\alpha(\hat{\mathbf{k}})Z_\beta(\hat{\mathbf{k}}')}\langle h_{\alpha\alpha_N}(\Omega_{\mathbf{k}},\Omega_{\mathbf{k}'})\rangle_N$$

$$\times \left\langle \exp\!\left(-i\mathbf{K}\cdot\sum_p\mathbf{R}_p\right)\right\rangle_N$$

$$\times \langle h_{\alpha\alpha_N}(\Omega_{\mathbf{k}},\,\Omega_{\mathbf{k}'})\rangle_N,\qquad\text{(B17)}$$

measuring the energy response for paths of N steps, where

$$h_{\alpha\beta}(\Omega,\,\Omega') = \delta_{\alpha\beta}\delta(\Omega-\Omega').\qquad\text{(B18)}$$

The approximation in the last step of relation (B17) involves the neglect of fluctuations with decay times that are rapid compared with diffusion times. The average

$$\langle h_{\alpha\alpha_N}(\Omega_{\mathbf{k}}-\Omega_{\mathbf{k}_N})\rangle_N = \frac{n_\alpha{}^3(\hat{\mathbf{k}})Z_\alpha(\hat{\mathbf{k}})}{(4\pi)^2[B]_n}\qquad\text{(B19)}$$

can be evaluated with the first form of Eqs. (B13) and (B5). $\Phi_{\hat{\mathbf{k}}\hat{\mathbf{k}}'}{}^{\alpha\beta}(\mathbf{K},\,\Omega,\,t)$ is evaluated as the sum over N of $\Phi_{\hat{\mathbf{k}}\hat{\mathbf{k}}'}{}^{N,\alpha\beta}(\mathbf{K},\,\Omega,\,t)$, which one obtains from relation (B17) by replacing $\langle\exp(-i\mathbf{K}\cdot\Sigma_p\mathbf{R}_p)\rangle_N$ with $\Phi^N(\mathbf{K},\,\Omega,\,t)$ in Eq. (2.5.14). The result, Eq. (2.5.43), follows directly from relations (B17) and (B19) and from Eq. (2.5.20) relating $\langle T\rangle$ to $[B]_n$.

APPENDIX C: CALCULATION OF $\langle R_z{}^2\rangle$, $\langle R_x{}^2\rangle$

In this appendix we outline a method for calculating the mean-square displacements per step, $\langle R_z{}^2\rangle$ and $\langle R_x{}^2\rangle$. Once these have been calculated, the parallel and the perpendicular diffusion coefficients can be calculated by means of Eqs. (2.5.26). The complex steps in these calculations are facilitated by the introduction of some additional formalism. In particular, the Dirac bra and ket formalism of quantum mechanics is extremely useful. We introduce the ket

$$|1\rangle = |\Omega_{\mathbf{k}_1},\,\alpha_1\rangle,\qquad\text{(C1)}$$

specifying the state with a photon of polarization α_1 propagating with phase velocity in the directions $\Omega_{\mathbf{k}_1}$. Matrix operators can be expressed in the usual way in terms of their matrix elements with the above kets and their associated bras. For example,

$$B(1,\,2) = B_{\alpha_1,a_2}(\hat{\mathbf{k}}_1,\,\hat{\mathbf{k}}_2) = \langle 1|B|2\rangle.\qquad\text{(C2)}$$

The integrands for probability path integrals defined in Eqs. (B9) and (B14) always involve a factor $n^3(1)$. Because of this, it is useful to define the unit operator with an $n^3(1)$ weight:

$$1 = \int \mathrm{d}1|1\rangle n^3(1)\langle 1|$$

$$= \sum_{\alpha_1}\int \mathrm{d}\Omega_{\mathbf{k}_1}|\Omega_{\mathbf{k}_1},\,\alpha_1\rangle n_{\alpha_1}{}^3(\hat{\mathbf{k}}_1)\langle\Omega_{\mathbf{k}_1},\,\alpha_1|,\quad\text{(C3)}$$

and orthogonality by means of

$$\langle 1|2\rangle = \frac{\delta(1-2)}{n^3(1)} = \frac{\delta(\theta_{\mathbf{k}_1}-\theta_{\mathbf{k}_2})\delta(\phi_{\mathbf{k}_1}-\phi_{\mathbf{k}_2})}{\sin\theta_{\mathbf{k}_1}n_{\alpha_1}{}^3(\mathbf{k}_1)}.\qquad\text{(C4)}$$

Matrix elements, inner products, and matrix elements of operator products then follow. A function $g_{\alpha_1}(\Omega_{\mathbf{k}_1})$ of $1 = (\Omega_{\mathbf{k}_1},\,\alpha_1)$ can be expressed as

$$g_{\alpha_1}(\Omega_{\mathbf{k}_1}) = g(1) = \langle 1|g\rangle.\qquad\text{(C5)}$$

The inner product of two functions f and g is

$$\langle f|g\rangle = \int \mathrm{d}1 f(1)n^3(1)g(1),\qquad\text{(C6)}$$

and the $1-1'$ matrix element of the product of two operators A and B is

$$\langle 1|AB|1'\rangle = \int \mathrm{d}2\langle 1|A|2\rangle n^3(2)\langle 2|B|1'\rangle.\qquad\text{(C7)}$$

The matrix elements of an operator A and its inverse A^{-1} satisfy

$$\int \mathrm{d}2\langle 1|A^{-1}|2\rangle n^3(2)\langle 2|A|1'\rangle = \langle 1|1'\rangle.\qquad\text{(C8)}$$

With a few more definitions, we can express $\langle R_i{}^2\rangle$ in a compact operator form. First, we define the operators

$$\widetilde{Z}^{-1}(2,\,1) = \frac{1}{Z(1)}\frac{\delta(2-1)}{n^3(1)},\qquad\text{(C9)}$$

$$\tilde{\pi}(2, 1) = \frac{B(3, 1)}{Z(1)} = \langle 2|B\tilde{Z}^{-1}|1\rangle. \qquad (C10)$$

Then

$$\tilde{Z}(1, 2) = Z(1)\delta(1 - 2)/n^3(1). \qquad (C11)$$

The matrix elements of the nth power of the ith component of the mean free displacement per step is

$$\langle 1|(l_i')^n\rangle = [l_{\alpha_1}(\hat{\mathbf{k}}_1)e_{g\alpha_1,i}(\hat{\mathbf{k}}_1)/\cos \delta_{\alpha_1}(\hat{\mathbf{k}}_1)]^n, \quad (C12)$$

where $\mathbf{e}_{g\alpha}(\hat{\mathbf{k}})$ is the unit vector along the group velocity with polarization α, which is equal to $\hat{\mathbf{k}}$ when $\alpha = 2$ and is given by Eq. (2.2.19) when $\alpha = 1$. With these definitions it is straightforward with the aid of Eq. (B14) to show that the mean-square displacement for a given bond satisfies

$$(4\pi)^2[B]_n\langle R_{pi}^2\rangle = 2\langle(l_i')^2|B|c\rangle, \qquad (C13)$$

where $|c\rangle$ is the uniform state, with $\langle 1|c\rangle = 1$ being independent of $\Omega_{\mathbf{k}_1}$ and α_1. Similarly,

$$\langle R_{ni}R_{mi}\rangle = \langle l_i'|\tilde{\pi}^{n-m-1}B|l_i'\rangle, \qquad (C14)$$

$$\frac{1}{N}\sum_{n>m}\langle R_{ni}R_{mi}\rangle = \langle l_i'|(1 - \tilde{\pi})^{-1}B|l_i'\rangle$$
$$= \langle l_i'|\tilde{Z}(\tilde{Z} - B)^{-1}B|l_i'\rangle. \qquad (C15)$$

The final matrix element in Eq. (C13) can be reexpressed as

$$\langle(l_i')^2|B|c\rangle = \int d1d2l_i'^2(1)n^3(1)B(1, 2)n^3(2)$$

$$= \int d1l_i'^2(1)n^3(1)Z(1)$$

$$= \int d1d2l_i'(1)n^3(1)\tilde{Z}(1, 2)n^3(2)l_i'(2)$$

$$= \langle l_i'|\tilde{Z}|l_i'\rangle, \qquad (C16)$$

where we used Eqs. (B5) and (C11): Combining Eqs. (C13), (C14), (C16), and (2.5.16), we obtain

$$(4\pi)^2[B]_n\langle R_i^2\rangle = 2\langle l_i'|\tilde{Z} + \tilde{Z}(\tilde{Z} - B)^{-1}B|l_i'\rangle$$
$$= 2\langle l_i'|\tilde{Z}(\tilde{Z} - B)^{-1}\tilde{Z}|l_i'\rangle$$
$$= 2\langle g_i|(\tilde{Z} - B)^{-1}|g_i\rangle, \qquad (C17)$$

where

$$\langle 1|g_i\rangle = l_i'(1)Z(1) = \frac{(4\pi)^2}{n(1)\cos \delta(1)}e_{g,i}(1). \quad (C18)$$

Using Eqs. (2.2.19) and (2.2.21), we obtain

$$\langle 1|g_z\rangle = \frac{(4\pi)^2 \cos \theta_{\mathbf{k}_1}}{n_2}\begin{pmatrix}\tilde{n}_1(\hat{\mathbf{k}}_1)\\1\end{pmatrix}, \qquad (C19)$$

$$\langle 1|g_x\rangle = \frac{(4\pi)^2 \sin \theta_{\mathbf{k}_1} \cos \phi_{\mathbf{k}_1}}{n_2}\begin{pmatrix}(\epsilon_\perp/\epsilon_\parallel)\tilde{n}_1(\hat{\mathbf{k}}_1)\\1\end{pmatrix},$$
$$(C20)$$

where

$$\tilde{n}_1(\hat{\mathbf{k}}) = \frac{n_1(\hat{\mathbf{k}})}{n_2} = \left(\frac{1 + \eta}{1 + \eta \cos^2 \theta_{\mathbf{k}}}\right)^{1/2}, \qquad (C21)$$

$$\eta = \Delta\epsilon/(\epsilon_\perp). \qquad (C22)$$

Equation (C17) provides a formally complete expression for the displacement $\langle R_i^2\rangle$. Unfortunately, the inverse of the operator

$$\mathcal{B} = \tilde{Z} - B \qquad (C23)$$

cannot be calculated exactly, and we must resort to some approximation scheme to calculate $\langle R_i^2\rangle$. The most direct approach for evaluating $\mathcal{B}^{-1}$ is to find the matrix elements of $\mathcal{B}$ in some appropriate basis and take its matrix inverse. We need only a particular matrix element (the g_i-g_i element) of $\mathcal{B}^{-1}$, and for approximation purposes it is useful to choose a basis set with the state $|g_i\rangle$ proportional to one of its members. For the ordinary polarization, the normal spherical harmonic basis set satisfies the above criterion. For the extraordinary rays, formal properties of the reduced index of refraction $\tilde{n}_1(\mathbf{k})$ allow us to construct a basis set with the desired properties from the spherical harmonic set. To this end, we define

$$C_{\mathbf{k}} = \tilde{n}_1(\hat{\mathbf{k}})\cos \theta_{\mathbf{k}},$$
$$S_{\mathbf{k}} = \tilde{n}_1(\hat{\mathbf{k}})\sin \theta_{\mathbf{k}} = (1 + \eta)\sqrt{1 - C_{\mathbf{k}}^2}. \qquad (C24)$$

Using Eq. (2.2.14), we can show that

$$(1 + \eta)dC_{\mathbf{k}} = \tilde{n}_1^3(\hat{\mathbf{k}})d(\cos \theta_{\mathbf{k}}), \qquad (C25)$$

so that

$$\int d\Omega_{\mathbf{k}}n_1^3(\hat{\mathbf{k}}) = (1 + \eta)n_2^3\int dC_{\mathbf{k}}d\phi_{\mathbf{k}}. \qquad (C26)$$

Thus a complete set of orthonormal states relative to the unit operator defined in Eq. (C3) is

$$\langle\Omega_{\mathbf{k}}\alpha|lm\beta\rangle = \delta_\alpha^\beta \frac{1}{n_2^{3/2}}\frac{1}{(1 + \eta_\alpha)^{1/2}}Y_{lm}(C_{\mathbf{k},\alpha}, \phi_{\mathbf{k}}),$$
$$(C27)$$

where $\eta_1 = \eta$, $\eta_2 = 1$, $C_{\mathbf{k},1} = C_{\mathbf{k}}$, $C_{\mathbf{k},2} = \cos \theta_{\mathbf{k}}$, and $Y_{lm}(\cos \theta, \phi)$ is the spherical harmonic expressed as a function of $\cos \theta$ and ϕ rather than as a function of θ and ϕ. It is more convenient for us to use the vector rather than complex spherical harmonics for $l = 1$, i.e., to use $|z\rangle = |l = 1$, $m = 0\rangle$, $|x\rangle = (|1, 1\rangle + |1, -1\rangle)/\sqrt{2}$, and $|y\rangle = (|1, 1\rangle + |1, -1\rangle)/(\sqrt{2}i)$ rather than the set $|1, m\rangle$. Then

$$\langle\Omega_{\mathbf{k}}\alpha|z\beta\rangle = \delta_\alpha^\beta \frac{1}{n_2^{3/2}}\frac{1}{(1 + \eta_\alpha)^{1/2}}\sqrt{\frac{3}{4\pi}}C_{\mathbf{k},\alpha},$$

$$\langle\Omega_{\mathbf{k}}\alpha|x\beta\rangle = \delta_\alpha^\beta \frac{1}{n_2^{3/2}}\frac{1}{(1 + \eta_\alpha)^{1/2}}\sqrt{\frac{3}{4\pi}}$$
$$\times \sqrt{1 - C_{\mathbf{k},\alpha}^2}\cos \phi_{\mathbf{k}}, \qquad (C28)$$

and $\langle\mu\alpha|\nu\beta\rangle = \delta_{\mu\nu}\delta_{\alpha\beta}$ for $\mu, \nu = x, z$. From this and Eqs. (C19) and (C20), we obtain

$$\langle z\beta|g_z\rangle = (4\pi)^2\sqrt{n_2}\sqrt{4\pi/3}\sqrt{1 + \eta},$$
$$\langle x\beta|g_x\rangle = (4\pi)^2\sqrt{n_2}\sqrt{4\pi/3}, \qquad (C29)$$

$$\langle z\beta|g_x\rangle = \langle x\beta|g_z\rangle = 0. \tag{C30}$$

To find an approximate expression for $\langle R_z{}^2\rangle$ and $\langle R_x{}^2\rangle$, we restrict ourselves to the subspace spanned by $|z\alpha\rangle$ and $|x\alpha\rangle$. There are no x–z cross terms in the $\mathcal{B}$ matrix. In addition,

$$\langle\mu\alpha|\mathcal{B}|\mu\beta\rangle = n_2{}^3\,\frac{3}{4\pi}\begin{bmatrix}(1+\eta)\mathcal{B}_{11}{}^\mu & \sqrt{1+\eta}\mathcal{B}_{12}{}^\mu \\ \sqrt{1+\eta}\mathcal{B}_{21}{}^\mu & \mathcal{B}_{22}{}^\mu\end{bmatrix}, \tag{C31}$$

where

$$\mathcal{B}_{\alpha\beta}^z = \int \mathrm{d}C\mathrm{d}C'\mathrm{d}\phi\mathrm{d}\phi'\,C\mathcal{B}_{\alpha\beta}C', \tag{C32}$$

$$\mathcal{B}_{\alpha\beta}^x = \int \mathrm{d}C\mathrm{d}C'\mathrm{d}\phi\mathrm{d}\phi'\,\sqrt{1-C^2}\mathcal{B}_{\alpha\beta}\sqrt{1-C^{2\prime}} \tag{C33}$$

Equations (C32) and (2.5.37), respectively, reduce to Eqs. (2.5.37) and (2.5.38) with the aid of Eqs. (C23), (C11), and (B5). From this, we can calculate

$$\langle R_z{}^2\rangle = 2\langle g_z|z\alpha\rangle\langle z\beta|\mathcal{B}^{-1}|z\beta\rangle\langle z\beta|g_z\rangle$$
$$= 2\left(\frac{4\pi}{3}\right)^2\frac{(4\pi)^2}{n_2{}^2[B]_n}\frac{\mathcal{B}_{11}{}^z + \mathcal{B}_{22}{}^z - 2\mathcal{B}_{12}{}^z}{\det\mathcal{B}^z}, \tag{C34}$$

$$\langle R_x{}^2\rangle = \langle g_z|z\alpha\rangle\langle z\beta|\mathcal{B}^{-1}|z\beta\rangle\langle z\beta|g_z\rangle = 2\left(\frac{4\pi}{3}\right)^2\frac{(4\pi)^2}{n_2{}^2[B]_n}$$
$$\times\frac{(1+\eta)\mathcal{B}_{11}{}^z + \mathcal{B}_{22}{}^z - 2\sqrt{1+\eta}\mathcal{B}_{12}{}^z}{(1+\eta)\det\mathcal{B}^z}, \tag{C35}$$

where $\det\mathcal{B}^\mu = \mathcal{B}_{11f}{}^\mu\mathcal{B}_{22}{}^\mu - \mathcal{B}_{12}{}^\mu\mathcal{B}_{21}{}^\mu$. Note that both $\langle R_x{}^2\rangle$ and $\langle R_x{}^2\rangle$ are proportional to $[B]_n$, which diverges as $H\to 0$. The factors following $[B]_n^{-1}$ in these expressions are well behaved in the zero-field limit. Thus both mean-square displacements tend to zero as $H\to 0$ in the same way that the average time $\langle T\rangle$ and the average mean free path $\bar{l}$ tend to zero. Combining Eqs. (C34) and (C35) with Eq. (2.5.20), we obtain Eqs. (2.5.36) for $D_\parallel$ and $D_\perp$.

APPENDIX D: STRUCTURE FACTOR

We give the two important structure factors $B_{12}(\hat{\mathbf{k}},\hat{\mathbf{q}})$ and $B_{11}(\hat{\mathbf{k}},\hat{\mathbf{q}})$ in the coordinates $C_{\mathbf{k}}$, $S_{\mathbf{k}}$, $C_{\mathbf{q}}$, $S_{\mathbf{q}}$ and $\varphi = \phi - \phi'$, which we introduced in Appendix C. The parameters are the dielectric anisotropy $\eta = \Delta\epsilon/\epsilon_\perp$, the scaled Frank constants $\bar{K}_1 = K_1/K_3$ and $\bar{K}_2 = K_2/K_3$, and the scaled magnetic field $h = n_2\omega/c\sqrt{K_3/\Delta\chi}$:

$$B_{12}(\hat{\mathbf{k}},\hat{\mathbf{q}}) = \frac{\omega^2}{c^2}\frac{(\Delta\varepsilon)^2 k_B T}{K_3 n_2{}^6(1+\eta)^2}\frac{S_{\mathbf{k}}{}^2}{Q_\perp{}^2}\left[\frac{S_{\mathbf{k}}{}^2\sin^2\varphi}{\bar{K}_1 Q_\perp{}^2 + Q_\parallel{}^2 + h^2}\right.$$
$$\left.+\frac{(S_{\mathbf{k}}\cos\varphi - S_{\mathbf{q}})^2}{\bar{K}_2 Q_\perp{}^2 + Q_\parallel{}^2 + h^2}\right], \tag{D1a}$$

$$B_{11}(\hat{\mathbf{k}},\hat{\mathbf{q}}) = \frac{\omega^2}{c^2}\frac{(\Delta\varepsilon)^2 k_B T}{K_3 n_2{}^6(1+\eta)^2}\frac{1}{Q_\perp{}^2}$$
$$\times\left[\frac{\cos^2\varphi\,N_1 + 2\cos\varphi\,N_2 + N_3}{\bar{K}_1 Q_\perp{}^2 + Q_\parallel{}^2 + h^2}\right.$$
$$\left.+\frac{\sin^2\varphi\,N_4}{\bar{K}_2 Q_\perp{}^2 + Q_\parallel{}^2 + h^2}\right], \tag{D1b}$$

with

$$Q_\parallel{}^2 = (C_{\mathbf{k}} - C_{\mathbf{q}})^2, \quad Q_\perp{}^2 = S_{\mathbf{k}}{}^2 - 2S_{\mathbf{k}}S_{\mathbf{q}}\cos\varphi + S_{\mathbf{q}}{}^2, \tag{D2}$$

$$N_1 = (S_{\mathbf{k}}{}^2 C_{\mathbf{q}} - S_{\mathbf{q}}{}^2 C_{\mathbf{k}})^2, \quad N_2 = S_{\mathbf{k}}S_{\mathbf{q}}(S_{\mathbf{k}}{}^2 C_{\mathbf{q}} - S_{\mathbf{q}}{}^2 C_{\mathbf{k}})$$
$$\times(C_{\mathbf{k}} - C_{\mathbf{q}}),$$

$$N_3 = S_{\mathbf{k}}{}^2 S_{\mathbf{q}}{}^2(C_{\mathbf{k}} - C_{\mathbf{q}})^2, \quad N_4 = (S_{\mathbf{k}}{}^2 C_{\mathbf{q}} + S_{\mathbf{q}}{}^2 C_{\mathbf{k}})^2. \tag{D3}$$

REFERENCES AND NOTES

1. Y. Kuga and A. Ishimaru, "Retroreflectance from a dense distribution of spherical particles," J. Opt. Soc. Am. A **1**, 831–835 (1984); M. P. van Albada and A. Lagendijk, "Observation of weak localization of light in a random medium," Phys. Rev. Lett. **55**, 2692–2695 (1985); P. E. Wolf and G. Maret, "Weak localization and coherent backscattering of photons in disordered media," Phys. Rev. Lett. **55**, 2696–2699 (1985); S. Etemad, R. Thompson, and M. J. Andrejco, "Weak localization of photons: universal fluctuations and ensemble averaging," Phys. Rev. Lett. **57**, 575–578 (1986); M. Kaveh, M. Rosenbluh, I. Edrei, and I. Freund, "Weak localization and light scattering from disordered solids," Phys. Rev. Lett. **57**, 2049–2052 (1986); S. Etemad, "Weak localization of photons: termination of coherent random walks by absorption and confined geometry," Phys. Rev. Lett. **59**, 1420–1423 (1987); M. Rosenbluh, I. Edrei, M. Kaveh, and I. Freund, "Precision determinations of the line shape for coherently backscattered light from disordered solids: comparison of vector and scalar theories," Phys. Rev. A **35**, 4458–4460 (1987); E. Akkermans and R. Maynard, "Weak localization of waves," J. Phys. (Paris) Lett. **46**, L-1045–L-1053 (1985); E. Akkermans, P. E. Wolf, and R. Maynard, "Coherent backscattering of light by disordered media: analysis of the peak line shape," Phys. Rev. Lett. **56**, 1471–1474 (1986); M. J. Stephen and G. Cwilich, "Rayleigh scattering and weak localization: effects of polarization," Phys. Rev. B **34**, 7564–7572 (1986); M. B. van der Mark, M. P. van Albada, and A. Lagendijk, "Light scattering in strongly scattering media: multiple scattering and weak localization," Phys. Rev. B **37**, 3575–3592 (1988); E. Akkermans, P. E. Wolf, R. Maynard, and G. Maret, "Theoretical study of the coherent backscattering of light by disordered media," J. Phys. (Paris) **49**, 77–98 (1988); F. C. MacKintosh and S. John, "Coherent backscattering of light in the presence of time-reversal-noninvariant and parity-nonconserving media," Phys. Rev. B **37**, 1884–1897 (1988).
2. A. A. Golubentsev, "Suppression of interference effects in multiple scattering of light," Sov. Phys. JETP **59**, 26–32 (1984).
3. S. Feng and P. A. Lee, "Mesoscopic conductors and corrections in laser speckle patterns," Science **251**, 633–639 (1991); N. Garcia and A. Z. Genack, "Crossover to strong intensity correlation for microwave radiation in random media," Phys. Rev. Lett. **63**, 1678–1681 (1989); M. P. van Albada, J. F. de Boer, and A. Lagendijk, "Observation of long-range intensity correlation in the transport of coherent light through a random medium," Phys. Rev. Lett. **64**, 2787–2790 (1990).

4. A. Genack and N. Garcia, "Observation of photon localization in a three-dimensional disordered system," Phys. Rev. Lett. **66**, 2064–2067 (1991); S. John, "Localization of light," Phys. Today **41**, 32–40 (1991); Scattering and localization of classical waves in random media, P. Sheng, ed. (World Scientific, Singapore, 1990).

5. E. Yablonovitch and T. J. Gmitter, "Photonic band structure: the face-centered-cubic case," Phys. Rev. Lett. **63**, 1950–1953 (1987).

6. N. M. Lawandy, R. Balachandran, A. Gomes, and E. Sauvin, "Laser action in strongly scattering media," Nature (London) **368**, 436–438 (1994); D. S. Wierswa, M. P. Vanalbada, and A. Lagendijk, "Coherent backscattering of light from amplifying random media," Phys. Rev. Lett. **75**, 1739–1742 (1995).

7. D. J. Pine, D. A. Weitz, G. Maret, P. E. Wolf, E. Herbolzheimer, and P. M. Chaikin, "Dynamical correlations of multiply scattered light," in *Scattering and Localization of Classical Waves in Random Media,* P. Sheng, ed., Vol. 8 of Directions in Condensed Matter Physics (World Scientific, Singapore, 1990), pp. 312–372.

8. F. C. MacKintosh and S. John, "Diffusing-wave spectroscopy and multiple scattering of light in correlated random media," Phys. Rev. B **40**, 2383–2406 (1989).

9. G. Maret and P. E. Wolf, "Multiple light scattering from disordered media. The effect of Brownian motion of scatterers," Z. Phys. B **65**, 409–413 (1987); M. Rosenbluh, M. Hoshen, I. Freund, and M. Kaveh, "Time evolution of universal optical fluctuations," Phys. Rev. Lett. **58**, 2754–2757 (1987); D. J. Pine, D. A. Weitz, P. M. Chaikin, and E. Herbolzheimer, "Diffusing-wave spectroscopy," Phys. Rev. Lett. **60**, 1134–1137 (1988); M. J. Stephen, "Temporal fluctuations in wave propagation in random media," Phys. Rev. B **37**, 1–5 (1988).

10. M. H. Kao, A. G. Yodh, and D. J. Pine, "Observation of Brownian motion on the time scale of hydrodynamic interactions," Phys. Rev. Lett. **70**, 242–245 (1993); P. D. Kaplan, A. G. Yodh, and D. J. Pine, "Diffusion and structure in dense binary suspensions," Phys. Rev. Lett. **68**, 393–396 (1992); A. J. C. Ladd, H. Gang, J. X. Zhu, and D. A. Weitz, "Time-dependent collective diffusion of colloidal particles," Phys. Rev. Lett. **74**, 318–321 (1995); S. J. Nilsen and A. P. Gast, "The influence of structure on diffusion in screened Coulombic suspensions," J. Chem. Phys. **101**, 4975–4985 (1994); X. Qiu, X. L. Wu, J. Z. Xue, D. J. Pine, D. A. Weitz, and P. M. Chaikin, "Hydrodynamic interactions in concentrated suspensions," Phys. Rev. Lett. **65**, 516–519 (1990); D. A. Weitz, D. J. Pine, P. N. Pusey, and R. J. A. Tough, "Nondiffusive Brownian motion studied by diffusing-wave spectroscopy," Phys. Rev. Lett. **63**, 1747–1750 (1989); J. X. Zhu, D. J. Durian, J. Muller, D. A. Weitz, and D. J. Pine, "Scaling of transient hydrodynamic interactions in concentrated suspensions," Phys. Rev. Lett. **68**, 2559–2562 (1992).

11. D. J. Durian, D. A. Weitz, and D. J. Pine, "Multiple light-scattering probes of foam structure and dynamics," Science **252**, 686–688 (1991); A. D. Gopal and D. J. Durian, "Nonlinear bubble dynamics in a slowly driven foam," Phys. Rev. Lett. **75**, 2610–2613 (1995).

12. H. Gang, A. H. Krall, and D. A. Weitz, "Shape fluctuations of interacting fluid droplets," Phys. Rev. Lett. **73**, 3435–3458 (1994).

13. D. G. Dalgleish and D. S. Horne, "Studies of gelation of acidified and renneted milks using diffusing-wave spectroscopy," Milchwissenschaft **46**, 417–424 (1991); P. D. Kaplan, A. G. Yodh, and D. F. Townsend, "Noninvasive study of gel formation in polymer-stabilized dense colloids using multiply scattered light," J. Colloid Interface Sci. **155**, 319–324 (1993).

14. D. A. Boas, L. J. Campbell, and A. G. Yodh, "Scattering and imaging with diffusing temporal correlations," Phys. Rev. Lett. **75**, 1855–1859 (1995).

15. M. Cutler, "Transillumination as an aid in the diagnosis of breast lesions, with special reference to its value in cases of bleeding nipple," Surg. Gynecol. Obstet. **49**, 508–512 (1929).

16. A. G. Yodh and B. Chance, "Spectroscopy and imaging with diffusing light," Phys. Today **48**, 34–40 (1995); B. Chance and R. R. Alfano, eds., *Optical Tomography: Photon Migration, and Spectroscopy of Tissue and Model Media: Theory, Human Studies, and Instrumentation*, Proc. SPIE **2389** (1995).

17. M. S. Patterson, B. Chance, and B. C. Wilson, "Time resolved reflectance and transmittance for the noninvasive measurement of tissue optical properties," Appl. Opt. **28**, 2331–2336 (1989); M. S. Patterson, J. D. Moulton, B. C. Wilson, K. W. Berndt, and J. R. Lakowicz, "Frequency-domain reflectance for the determination of the scattering and absorption properties of tissue, " Appl. Opt. **30**, 4474–4478 (1991).

18. E. Gratton, W. Mantulin, M. J. van de Ven, J. Fishkin, M. Maris, and B. Chance, in *Proceedings of the Third International Conference: Peace through Mind/Brain Science*, August 5–10, 1990 (Hamamatsu Corp., Hamamatsu, Japan, 1990), pp. 183–189.

19. D. A. Benaron and D. K. Stevenson "Optical time of flight and absorbance imaging of biologic media," Science **259**, 1463–1466 (1993); D. T. Delpy, M. Cope, P. van de Zee, S. Arridge, S. Wray, and J. Wyatt, "Estimation of optical pathlength through tissue from direct time of flight measurement," Phys. Med. Biol. **33**, 1433–1442 (1988); S. L. Jacques, "Time resolved propagation of ultrashort laser pulses within turbid tissues," Appl. Opt. **28**, 2223–2229 (1989); M. S. Patterson, B. Chance, and B. C. Wilson, "Time resolved reflectance and transmittance for the noninvasive measurement of tissue optical properties," Appl. Opt. **28**, 2331–2336 (1989).

20. D. A. Boas, M. A. O'Leary, B. Chance, and A. G. Yodh, "Scattering and wavelength transduction of diffuse photon density waves," Phys. Rev. E **47**, R2999–R3003 (1993); M. A. O'Leary, D. A. Boas, B. Chance, and A. G. Yodh, "Refraction of diffuse photon density waves," Phys. Rev. Lett. **69**, 2658–2661 (1992).

21. J. Fishkin and E. Gratton, "Propagation of photon density waves in strongly scattering media containing an absorbing semi-infinite plane bounded by a straight edge," J. Opt. Soc. Am. A **10**, 127–140 (1993).

22. J. M. Schmitt, A. Knuttel, and J. R. Knudsen, "Interference of diffusive light waves," J. Opt. Soc. Am. A **9**, 1832–1843 (1992).

23. E. M. Sevick, J. Lakowicz, H. Szmacinski, K. Nowacyzk, and M. L. Johnson, "Frequency domain imaging of absorbers obscured by scattering," J. Photochem. Photobiol. B **16**, 169–185 (1992); B. Tromberg, L. O. Svaasand, T. T. Tsay, and R. C. Haskell, "Properties of photon density waves in multiple-scattering media," Appl. Opt. **32**, 607–616 (1993).

24. S. P. Gopinath, C. Roberston, and B. Chance, "Near-infrared spectroscopic localization of intracranial hematomas," J. Neurosurg. **79**, 43–47 (1993).

25. C. D. Kurth, J. M. Steven, and S. C. Nicolson, "Cerebral oxygenation during pediatric cardiac surgery using deep hypothermic circulatory arrest," Anesthesiology **82**, 74–82 (1995).

26. W. Bank and B. Chance, "An oxidative defect in metabolic myopathies: diagnosed by non-invasive tissue oximetry," Ann. Neurol. **36**, 830–837 (1994); W. Bank and B. Chance, "Diagnosis of mitochondrial disease by NIRS," in *Optical Tomography: Photon Migration, and Spectroscopy of Tissue and Model Media: Theory, Human Studies, and Instrumentation*, B. Chance and R. R. Alfano, eds., Proc. SPIE **2389**, 829–834; B. Chance and W. Bank, "Genetic disease of mitochondrial function evaluated by NMR and NIR spectroscopy of skeletal tissue," Biochim. Biophys. Acta **1271**, 7–14 (1995).

27. S. Fantini, M. A. Franceschini, G. Gaida, E. Gratton, H. Jess, W. M. Mantulin, K. T. Moesta, P. M. Schlag, and M. Kashke, "Frequency-domain optical mammography: edge effect corrections," Med. Phys. **23**, 1–9 (1996); M. A. Franceschini, K. T. Moesta, S. Fantini, G. Gaida, E. Gratton, H. Jess, M. Seeber, P. M. Schlag, and M. Kashke, "Frequency-domain techniques enhance optical mammography: initial clinical results," Proc. Natl. Acad. Sci. USA (to be published).

28. H. Stark and T. C. Lubensky, "Multiple light scattering in nematic liquid crystals," Phys. Rev. Lett. **77**, 2229–2232 (1996); M. H. Kao, K. A. Jester, A. G. Yodh, and P. J. Collings, Phys. Rev. Lett. **77**, 2233–2236 (1996).

29. H. Stark and T. C. Lubensky, "Multiple light scattering in anisotropic random media," Phys. Rev. E (to be published).

30. P. G. de Gennes and J. Prost, *The Physics of Liquid Crystals*, 2nd ed. (Clarendon, Oxford, 1993).

31. S. Chandrasekhar, *Liquid Crystals*, 2nd ed. (Cambridge U. Press, Cambridge, 1992).

32. D. V. Vlasov, L. A. Zubkov, N. V. Orekhova, and V. P. Romanov, "Weak localization due to scattering of light in non-oriented liquid crystals," JETP Lett. **48**, 91–93 (1988) [Pis'ma Zh. Eksp. Teor. Fiz. **48**, 86–88 (1988)].

33. H. K. M. Vithana, L. Asfaw, and D. L. Johnson, "Coherent backscattering of light in a nematic liquid crystal," Phys. Rev. Lett. **70**, 3561–3564 (1993).

34. L. D. Landau and E. M. Lifschitz, *Electrodynamics of Continuous Media*, Vol. 8 of Course of Theoretical Physics, 1st English ed. (Pergamon, Oxford, 1960), Chap. 11.

35. M. Born and E. Wolf, *Principles of Optics*, 6th ed. (Pergamon, Oxford, 1980).

36. R. C. Haskell, L. O. Svaasand, T. Tsay, T. Feng, M. S. McAdams, and B. J. Tromberg, "Boundary conditions for the diffusion equations in radiative transfer," J. Opt. Soc. Am. A **11**, 2727–2741 (1994).

37. Here we neglect any biaxial fluctuations.

38. M. Lax and D. F. Nelson, in "Adventures in Green's land: light scattering in anisotropic media," in *Proceedings of the Third Rochester Conference on Coherence and Quantum Optics*, L. Mandel and E. Wolf, eds. (Plenum, New York, 1973), pp. 415–445.

39. Because we use a continuum of **q** vectors, the equipartition theorem gives $\langle \delta n_\delta(\mathbf{q}, 0) \delta n_\delta^*(\mathbf{q}', 0) \rangle = [k_B T/$

$K_\delta(\mathbf{q})] \delta(\mathbf{q} - \mathbf{q}')$. Then we set $\langle \delta n_\delta(\mathbf{q}, 0) \delta n_\delta^*(\mathbf{q}, 0) \rangle \equiv \int d^3 q/(2\pi)^3 \langle \delta n_\delta(\mathbf{q}, 0) \delta n_\delta^*(\mathbf{q}', 0) \rangle$.

40. D. Forster, T. C. Lubensky, P. C. Martin, J. Swift, and P. S. Pershan, "Hydrodynamics of liquid crystals," Phys. Rev. Lett. **26**, 1016–1019 (1971).

41. D. Langevin and M.-A. Bouchiat, "Anisotropy of the turbidity of an oriented nematic liquid crystal," J. Phys. (Paris) Colloq. **36**, C1-197–C1-202 (1975).

42. U. Frisch, in "Wave propagation in random media," in *Probabilistic Methods in Applied Mathematics*, A. T. Barucha-Reid, ed. (Academic, New York, 1968), Vol. 1, pp. 75–198.

43. Ping Sheng, *Introduction to Wave Scattering, Localization, and Mesoscopic Phenomena*, 1st ed. (Academic, San Diego, Calif., 1995).

44. S. Ramaswamy, "Multiple light scattering and photon diffusion in a nematic liquid crystal," J. Phys. C **98**, 9318–9321 (1994). This reference considers diffusive light transport in a nematic liquid crystal and derives an expression for the photon self-energy. Its evaluation of the photon mean free path is, however, incorrect in that it misses the logarithmic dependence on external magnetic field. It also does not calculate the transport mean free path.

45. D. A. Weitz and D. J. Pine, in "Diffusing-wave spectroscopy," in *Dynamic Light Scattering*, W. Brown, ed. (Oxford U. Press, Oxford, 1992), pp. 652–720.

46. A. Y. Val'kov and V. P. Romanov, "Characteristics of propagation and scattering of light in nematic liquid crystals," Sov. Phys. JETP **63**, 737–743 (1986) [Zh. Eksp. Teor. Fiz. **90**, 1264–1274 (1986)].

47. B. A. Tiggelen, R. Maynard, and A. Heiderich, "Anisotropic light diffusion in oriented nematic liquid crystals," Phys. Rev. Lett. **77**, 639–642 (1996).